Journal of Hydrology 572 (2019) 274–293

Contents lists available at ScienceDirect

Journal of Hydrology

journal homepage: www.elsevier.com/locate/jhydrol

Research papers

A salinity reactive transport and equilibrium chemistry model for regional-scale agricultural groundwater systems

Saman Tavakoli-Kivi*, Ryan T. Bailey, Timothy K. Gates

Department of Civil and Environmental Engineering, Colorado State University, 1372 Campus Delivery, Fort Collins, CO 80523-1372, United States

ARTICLE INFO

This manuscript was handled by Huaming Guo, Editor-in-Chief, with the assistance of Mingjie Chen, Associate Editor

Keywords:
Salinity
Groundwater
Reactive transport model
Equilibrium chemistry
Precipitation/dissolution
Irrigation

ABSTRACT

A three-dimensional coupled groundwater reactive transport and equilibrium chemistry model is presented that simulates the fate and transport of major salt ions in agricultural groundwater systems that span broad regions. The UZF-RT3D/SEC model amends the base model UZF-RT3D by coupling it with a new Salinity Equilibrium Chemistry (SEC) module to simulate the movement and transformation of major salt ions (calcium, magnesium, sodium, potassium, sulfate, chloride, bicarbonate, and carbonate) due to advection, dispersion, source/sink mixing, sulfur cycling, redox reactions, precipitation-dissolution, aqueous complexation, and cation exchange. The coupling procedure and the considered reactions make the model applicable for simulating regional-scale agricultural aquifer systems with data efficiency and an acceptable processing time. The model receives flow information from the MODFLOW-UZF flow model, which simulates variably-saturated groundwater flow in an efficient manner over regional scales. For use in agricultural areas, the model also accounts for crop uptake, soil organic matter decomposition, and mineralization/immobilization of carbon, nitrogen, and sulfur species. The model is applied to a salinity-impaired regional-scale (500 km^2) agricultural area within the irrigated valley of the Arkansas River in southeastern Colorado. It is calibrated and tested against salt ion groundwater concentrations measured in monitoring wells, soil salinity measurements from throughout the region, and total salt loads discharging from the aquifer to the stream network of the Arkansas River. Results indicate that the model represents well the overall magnitude and spatiotemporal trends of soil salinity and groundwater salinity in the aquifer, along with salt loading to streams, and therefore can be used to investigate best management practices for salt remediation. This, along with findings indicating that the inclusion of equilibrium chemistry is vital for producing the correct magnitude of salt ion concentrations and mass loadings, render a tool useful for regional investigation of other highly-salinized aquifer systems.

1. Introduction

High salinity in groundwater and soils afflicts many areas of the world, specifically arid and semi-arid agricultural regions that rely on irrigation for sustaining crop yield. Reduction in crop yield is an important economic consequence of salt build-up in the root zone in many regions of the world including Iran (Jalali, 2007; Jamshidzadeh et al., 2011; Ebrahimi et al, 2016), India (Singh, 2005; Jeevanandam et al., 2007; Misra et al., 2007; Lorenzen et al., 2012), the western United States (e.g. San Joaquin Valley in California, Schoups et al., 2006), Pakistan (Mahmood et al., 2001; Qureshi et al., 2008; Latif et al., 2009), China (Pereira et al. 2007; Chen et al, 2010; Wang et al. 2018), and Australia (Herczeg et al., 2001; Tweed et al., 2007; Skrzypek et al., 2013). High salinity can occur due to waterlogging from shallow groundwater with associated evaporative upflux (Morway and Gates, 2012; Harrington and Cook, 2014); dissolution of salt minerals such as gypsum ($CaSO_4$), calcite ($CaCO_3$), and halite (NaCl) (Harrington and Cook, 2014; Farid et al., 2015); and seawater intrusion in coastal areas (Shammas and Jacks, 2007; Sherif et al., 2011; Blanco et al., 2013).

The impact of possible remediation practices on high groundwater and soil salinity often is assessed using models that attempt to capture the major hydrologic processes and chemical reactions that govern the transport of salt species in coupled soil-aquifer systems. These models also are used to provide insights into the nature of processes that govern salt species transport in these systems. Models are employed at a variety of spatial scales, ranging from one-dimensional (1D) soil profiles to river basins, and include varying degrees of complexity, from simple advective transport to multi-species reactive transport integrating equilibrium and kinetic chemistry.

As summarized in Table 1, several models include many of the

* Corresponding author.
E-mail addresses: saman@colostate.edu (S. Tavakoli-Kivi), rtbailey@colostate.edu (R.T. Bailey), timothy.gates@colostate.edu (T.K. Gates).

https://doi.org/10.1016/j.jhydrol.2019.02.040
Received 5 December 2018; Received in revised form 19 February 2019; Accepted 21 February 2019
Available online 27 February 2019
0022-1694/

Table 1
Coupled transport and geochemical models (Steefel et al., 2015; Goncalves et al., 2006; Crawford, 1999).

Modeling code	Typical scale applicability	Advection/ Diffusion	Saturated Transport	Unsaturated Transport	1D/ 2D/3D	Sulfur Cycling	Redox Reaction	Complexation	Precipitation-dissolution	Ion Exchange	Adsorption Isotherms	Davis Activity	Debye-Huckel Activity
PHREEQC	Small	×	×		1D		×	×	×	×		×	×
UNSATCHEM	Small	×	×	×	2D			×	×	×		×	×
HYDRUS	Small	×	×	×	3D			×	×	×	?	×	×
HPx	Small	×	×	×	3D			×	×	×	?	×	×
HYDROGEOCHEM	Small	×	×	×	3D		×	×	×	×		×	×
UZF-RT3D/SEC	Small/Large	×	×	×	3D	×	×	×	×	×	×	×	×

?: unknown.

governing physical and chemical processes for salt fate and transport. PHREEQC is a 1D model developed to perform a variety of aqueous geochemical calculations in saturated media (Parkhust and Appelo, 1999). UNSATCHEM (Šimůnek and Suarez, 1994) includes chemical reactions such as precipitation-dissolution of salt minerals, cation exchange, and complexation to simulate spatio-temporal concentration of major salt ions in soil-water systems. HYDRUS-1D (Šimůnek et al., 2005), a finite element model for simulating the movement of water and multiple solutes in variably-saturated porous media, was amended to include the UNSATCHEM module for major salt ion chemistry (Šimůnek et al., 2012). Multidimensional modeling capability of HYDRUS has been developed as well. The HP1 model couples HYDRUS-1D with PHREEQC to address a broader range of ions but is restricted to 1D transport (Jacques et al., 2003, Jacques and Šimůnek, 2005). The second and third versions of HPx, were developed later to incorporate two-dimensional (2D) and three-dimensional (3D) modeling capability. HYDROGEOCHEM is a numerical fluid flow model which iteratively solves 3D fluid flow and geochemical transport equations (Yeh et al., 2004). For comparison, traits of the UZF-RT3D/SEC model presented here also are included in Table 1. Most notably, UZF-RT3D/SEC simulates all major salinity processes in a 3D variably-saturated groundwater flow system. Due to the linkage with MODFLOW, the model can also simulate salt mass exchange between the aquifer and surface water features (rivers, streams, lakes, reservoirs, etc).

Other models, besides those summarized in Table 1, link geochemistry and multi-species reactive transport in saturated or variably-saturated porous media [e.g. PHT3D, (Prommer et al., 2003); VAM2D, (Huyakorn et al., 1991); DYNAMIX (Narasimhan et al., 1986); PHAST (Parkhust et al., 2004); LEACHM (Wagenet and Hutson, 1987)]. However, they have not been applied to salt fate and transport and do not always include the necessary chemical reactions, e.g. cation exchange, or are limited to analysis of the saturated zone (e.g. PHAST, PHT3D). Moreover, these models typically are applied over small spatial scales, e.g. soil profiles at experimental field plots (Goncalves et al., 2006; Forkutsa et al., 2009; Tafteh and Sepaskhah, 2012; Rasouli et al., 2013), due to high computational costs and extensive data requirements.

A second subset of salinity models are those whose application at a large spatial scale (catchment to river basin) have been reported. Such tools are useful for the evaluation of agro-environmental health and economic vitality at a regional planning level; however, they may not include the chemical processes (e.g. precipitation-dissolution) that often govern salt ion concentration in variably-saturated groundwater systems or are computationally inefficient. Table 2 shows a list of salt transport modeling studies applied at the regional scale ($\sim 10^2$–10^3 km^2) and selected features of the respective model used for each study. The area of the study region and the modeled physical and chemical processes are included.

A hydro-salinity model that couples MODHMS with UNSATCHEM was used by Schoups et al. (2005) to simulate subsurface salt transport and storage in a 1400 km^2 region of the San Joaquin Valley. The coupling of the two models for 3D salinity reactive transport, however, is not explained in the paper, and the modeling system does not account for element (carbon, nitrogen, sulfur) mass cycling in the plant-soil system. Lin and Garcia (2008) applied WATSUIT, a steady-state model that calculates soil-water interaction in the root zone, in Colorado's Lower Arkansas River Valley to determine the salinity of deep percolation water. They modified WATSUIT to simulate dynamic conditions with a monthly time step and applied the model to simulate unsaturated flow for a 12-month period in the root zone of fields. SAHYSMOD (Oosterbaan, 2005) is an integrated agro-hydro-salinity model amenable to the analysis of large agricultural areas but handles processes based exclusively on water and salt balances and does not account for chemical reactions. SAHYSMOD has been applied to simulate the water and salt behavior in the semi-arid irrigated area of Haryana State in India where waterlogging and salinization have impacted the region for more than 40 years (Singh and Panda, 2012). Tuteja et al.,

Table 2
Salinity transport modeling studies applied at the regional scale.

Study area	Area of the study region	Model used	Simulated Salt species	Reference
San Joaquin Valley, California, USA	1400 km^2	Coupled MODHMS and UNSATCHEM	Gypsum and Calcite	Schoups et al. (2005)
Lower Arkansas River Valley, Colorado, USA	244 km^2	Modified WATSUIT	Gypsum, Calcite, and Magnesite	Lin and Garcia (2008)
Haryana State, India	920 km^2	SAHYSMOD	N/A	Singh et al. (2012)
Mandagery Creek Catchment, Australia	1668 km^2	CATSALT	N/A	Tuteja et al. (2003)
Lower Arkansas River Valley, Colorado, USA	500 km^2	MT3DMS + Water and Salt balance model for unsaturated zone	N/A	Burkhalter and Gates (2005, 2006)

(2003) assessed the effect of land use changes on salt and water balance in the Mandagery Creek catchment of New South Wales, Australia using CATSALT, a distributed water balance model linked with a salt transport module. Burkhalter and Gates (2005, 2006) developed and applied an MT3D model incorporating a one-dimensional mass balance in the unsaturated zone to simulate weekly soil and aquifer salt concentration across an irrigated region of Colorado's Lower Arkansas River Valley. The model assumed only advective transport, not accounting for kinetic and equilibrium chemical reactions. Tavakoli Kivi and Bailey (2017) simulated the groundwater fate and transport of SO_4 in the same region, but were not able to reproduce the correct magnitude of concentration in groundwater due to the neglect of equilibrium chemistry reactions (e.g. precipitation-dissolution of salt minerals) in the modeling framework.

Overall, the chemical processes that often regulate salt species' fate and transport, such as precipitation-dissolution, complexation, cation exchange, first-order degradation, and redox reactions have not been represented in modeling applications at a large spatial scale. Nevertheless, the degradation of aquifers and streams by the accumulation of salts, as well as their remediation, is brought about by practices and processes that interact from field to field over vast spatial extents. Models are needed that can adequately simulate these practices and processes to better understand salinization over regional landscapes and explore land and water management alternatives for mitigation. Moreover, there is a need to demonstrate in a data-rich environment the potential for such models to reasonably capture the major processes that determine the severity and distribution of salinity over a regional scale.

This study presents a finite-difference numerical model that simulates the fate and transport of major salt ions in large-scale variably-saturated groundwater systems while accounting for major salt inputs, equilibrium chemical reactions, oxidation-reduction reactions, and the cycling of carbon (C), nitrogen (N), and sulfur (S) in the plant-soil system. The modeling framework consists of groundwater flow modeling by MODFLOW and reactive transport modeling by UZF-RT3D (Bailey et al., 2013a) coupled with a new Salinity Equilibrium Chemistry (SEC) module. Processes simulated by MODFLOW include 1D flow in the unsaturated zone, evapotranspiration (ET) from crops and natural vegetation, groundwater pumping, canal seepage, 3D groundwater flow in the saturated zone, upflux through the vadose zone, and water exchange with streams (Morway et al., 2013). UZF-RT3D (Bailey et al., 2013a) is a finite-difference FORTRAN code that simulates reactive transport of multiple interacting chemical species in variably-saturated groundwater flow systems, using flow and source/sink output from the MODFLOW model. This paper presents UZF-RT3D/SEC, which allows the modeling framework to simulate the fate and transport of major salt ions [calcium (Ca), magnesium (Mg), sodium (Na), potassium (K), sulfate (SO_4), chloride (Cl), and bicarbonate (HCO_3)] in the aquifer system. Unique features of this framework include:

- The new SEC module, which simulates chemical equilibrium reactions for salt ions such as precipitation-dissolution of salt minerals (e.g. gypsum $CaSO_4$). In anticipation of model use in other regions worldwide, the salinity module source code has been designed for ease of including additional salt minerals that may be present in other groundwater systems.
- The use of MODFLOW's UZF (Unsaturated Zone Flow) package, which assumes vertical homogeneity of the unsaturated zone and neglects the diffusive term in the Richards equation, thus demanding less computational effort and data support than models that solve the full Richards equation; hence, providing a suitable tool for simulating variably-saturated flow and transport at the regional scale. To determine downward vertical flux, the kinematic wave approximation is used, with ET extracted from water stored within the soil root zone as a sink term within the equation. When a specified lower limit of readily-available soil water is reached, ET is

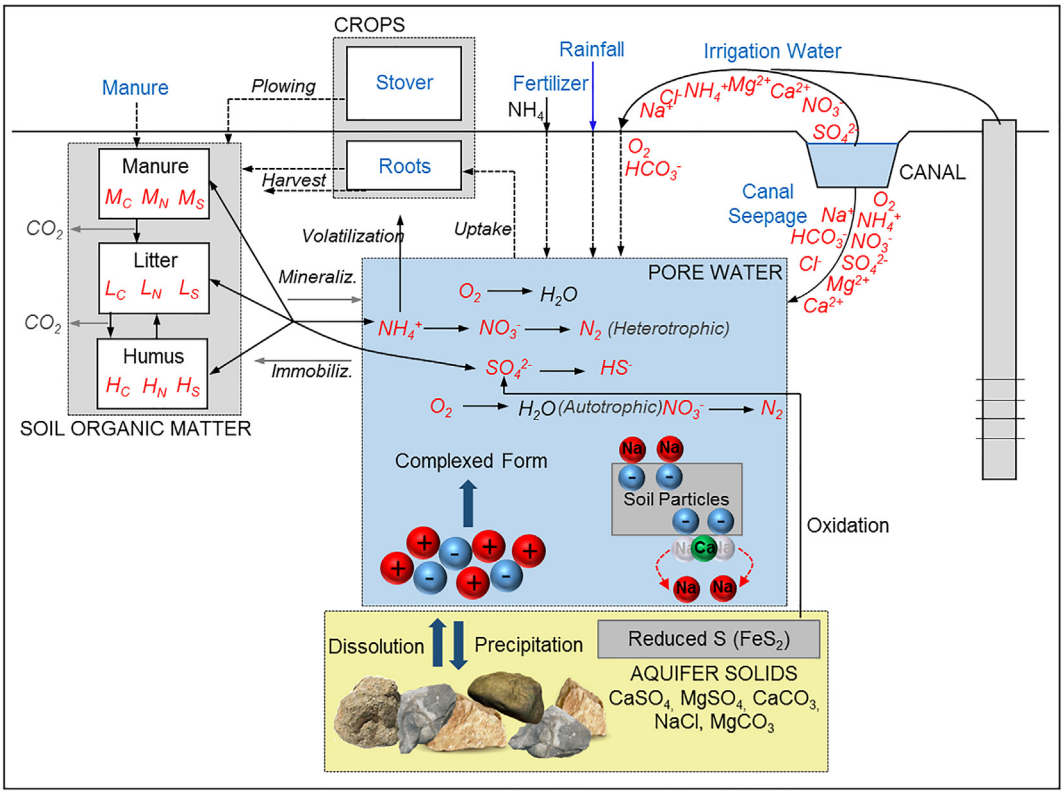

Fig. 1. Nutrient cycling and salt ion transport in the coupled soil-groundwater system in an agricultural area, including plant mass inputs/output, organic matter decomposition, mineralization/immobilization, oxidation-reduction reactions, precipitation-dissolution, complexation, and cation exchange.

then supplied by upflux from the water table, using a linear function of depth to the water table, up to a specified maximum extinction depth (Morway et al., 2013; Harbaugh, 2005).

– The use of C, N, and S cycling modules developed for UZF-RT3D (Bailey et al., 2013b; Tavakoli Kivi and Bailey, 2017). N cycling can affect SO_4 concentration in soil and groundwater due to redox sensitivity, and nitrate (NO_3) can oxidize SO_4 from shale material, which underlies many alluvial aquifers worldwide. These modules also include organic matter decomposition and mineralization, plant uptake, sorption, oxidation-reduction, and fertilizer loading.

2. Salinity fate and transport in an agricultural groundwater system

The fate and transport of major salt ions in an irrigated agricultural region are depicted in Fig. 1. The cycling of C and N are included (Bailey et al, 2013b) due to their effect on S cycling and SO_4 chemical reduction, and the release of SO_4 from pyrite (FeS_2) in the presence of O_2 and NO_3. These conditions are not present in all aquifer systems, but pyrite is present in bedrock and outcropped marine shale in many regions worldwide.

Cycling of S mass occurs as organic S is incorporated via plowing into soil organic matter, composed of litter (fast-decomposing) and humus (slow-decomposing), then mineralized to SO_4, and then taken up by crop roots during the growing season. S mass also can be added to the root zone via fertilizer. SO_4 can be chemically reduced via a microbially-mediated chemical reduction reaction (Frind et al., 1990), inhibited by the presence of O_2 and NO_3 due to the succession of terminal electron (e^-)-acceptor processes. Furthermore, SO_4 can be released from FeS_2 via autotrophic reduction of O_2 and NO_3 (Frind et al., 1990; Postma et al., 1991; Pauwels et al., 1998).

SO_4 mass, along with the mass of the other major anions (Cl, CO_3, HCO_3) and cations (Mg, Ca, Na), can be added to the subsurface via irrigation water and seeped surface water (canal water, stream water). Irrigation water can be derived either from surface water or from groundwater via pumping. If salt minerals, e.g. $CaSO_4$, $CaCO_3$, and NaCl, are present in the soil and aquifer sediments, dissolution of the salt solids or precipitation out of the solution can occur, resulting in an increase or decrease in salt ion concentration in the groundwater and soil water. In addition, complexation of the dissolved species and cation exchange reactions can occur. Once in the groundwater system, the salt ions can be transported through the aquifer and to surface water discharge sites. If concentrations exceed saturation limits, then precipitation to salt solids can occur.

3. Model development

The transport of m reactive species can be written in terms of concentrations, C_i, as (Miller and Benson, 1983; Steefel and Lasaga, 1994; Šimůnek and Suarez, 1994; Carrayrou et al., 2004; Ezzedine, 2015):

$$\frac{\partial C_i}{\partial t} = L(C_i, x, t) + f_j(C_1, ...,C_m) \quad (1)$$

where L denotes the transport model such as advection and diffusion and f_j represents the chemical sub-models such as precipitation/dissolution. This section describes the UZF-RT3D transport and chemical kinetics model, followed by a description of the new SEC module.

3.1. Salinity transport and chemical kinetics

The base solute reactive transport model is UZF-RT3D (Bailey et al., 2013b), which receives groundwater flow data from a MODFLOW-NWT (Niswonger et al., 2011) model that employs the Unsaturated-Zone Flow (UZF) package (Niswonger et al., 2006), and solves the following system of advection-dispersion-reaction (ADR) equations for the dissolved-phase species and the reaction equations for solid-phase species in variably-saturated groundwater systems using a finite-difference approach (Bailey et al., 2013a):

$$\frac{\partial(C_k\theta)}{\partial t}R_k = -\frac{\partial}{\partial x_i}(\theta v_i C_k) + \frac{\partial}{\partial x_i}\left(\theta D_{ij}\frac{\partial C_k}{\partial x_j}\right) + q_f C_{f_k} + \theta r_f - \rho_b\frac{\partial \bar{c}_k}{\partial t} - \rho_b\frac{\partial \bar{\bar{c}}_k}{\partial t} \quad k = 1, 2, ...,m \tag{2a}$$

$$\frac{\partial(C_l\varepsilon)}{\partial t} = \alpha_l P_S + \varepsilon r_s \quad l = 1, 2, ...,n \tag{2b}$$

where C_k and C_l are the concentration of the k^{th} dissolved-phase solute $[M_f L_f^{-3}]$ and l^{th} solid-phase species $[M_s L_s^{-3}]$ respectively, with f denoting the fluid phase; D_{ij} is the hydrodynamic dispersion coefficient $[L^2T^{-1}]$; v is the pore velocity $[L_b T^{-1}]$ with b denoting the bulk phase; θ is the volumetric water content $[L_f^3 L_b^{-3}]$; q_f is the volumetric flux of water representing sources and sinks $[L_f^3 T^{-1} L_b^{-3}]$ such as irrigation water, canal and seepage, groundwater discharge to the river, or pumped groundwater; C_f is the concentration of solute in the source or sink water $[M_f L_f^{-3}]$; r_f represents the rate of the reactions that occur in the dissolved phase $[M_f L_f^3 T^{-1}]$; R_j is the retardation factor for species j and is equal to $1 + (\rho_b K_{dj})/\theta$, where ρ_b is the bulk density of the porous media $[M_b L_b^{-3}]$ and K_{dj} is the partitioning coefficient for the jth species $[L_f^{-3} M_b]$; $\bar{c}_k$ is the total solid phase concentration of aqueous species k which considers precipitation/dissolution $[MM^{-1}]$; $\bar{\bar{c}}_k$ is the total exchanged phase concentration of aqueous species k $[MM^{-1}]$; P_S is the application rate of after-harvest stover mass [kg ha^{-1}]; α_l is the portion of the stover mass attributed to the solute; ε is the volumetric solid content $[L_s^3 L_b^{-3}]$ and is equal to $1 - \phi$, with ϕ representing porosity; and r_s is the reaction rate, with s denoting the solid phase. UZF-RT3D uses output from a MODFLOW-NWT (Niswonger et al., 2011) that uses the UZF package (Niwsonger et al., 2006) for v and q_f. Eq. (2b) represents change in soil organic matter (e.g. humus).

Using the form of the ADR equation in Eq. (2a), the transport of SO_4-S and Ca are written as follows, with the equations for the other major ions (Mg, Na, K, CO_3, HCO_3, Cl) similar to the Ca equation:

$$\frac{\partial(C_{SO_4-S}\theta)}{\partial t}R_{SO_4-S} = -\frac{\partial}{\partial x_i}(\theta v_i C_{SO_4-S}) + \frac{\partial}{\partial x_i}\left(\theta D_{ij}\frac{\partial C_{SO_4-S}}{\partial x_j}\right) + q_f C_{f_{SO_4-S}} + F_{SO_4-S} - U_{SO_4-S} + \varepsilon(r_{s,S}^{\min} - r_{s,S}^{imm}) + \theta(r_{f,SO_4-S}^{auto} - r_{f,SO_4-S}^{het}) - \rho_b\frac{\partial \bar{\bar{c}}_{SO_4-S}}{\partial t} \tag{3a}$$

$$\frac{\partial(C_{Ca}\theta)}{\partial t}R_{Ca} = -\frac{\partial}{\partial x_i}(\theta v_i C_{Ca}) + \frac{\partial}{\partial x_i}\left(\theta D_{ij}\frac{\partial C_{Ca}}{\partial x_j}\right) + q_f C_{f_{Ca}} - U_{Ca} - \rho_b\frac{\partial \bar{\bar{c}}_{Ca}}{\partial t} - \rho_b\frac{\partial \bar{c}_{Ca}}{\partial t} \tag{3b}$$

The SO_4-S transport equation is unique from the others in that it includes mineralization/ immobilization (due to S cycling), as well as microbially-mediated chemical reduction and autotrophic oxidation. Equations for S in the litter pool (L_S), in the humus pool (H_S), and in the manure pool (M_S) also are included in the UZF-RT3D model, but not shown here (see Tavakoli Kivi and Bailey, 2017). For the SO_4-S Eq. (3a), $F_{SO4\text{-}S}$ is the inorganic fertilizer application of S $[M_f L_b^{-3} T^{-1}]$; $U_{SO4\text{-}S}$ is the uptake rate $[M_f L_b^{-3} T^{-1}]$; *min* and *imm* signify mineralization and immobilization, respectively; and *auto* and *het* represent autotrophic and heterotrophic chemical reduction, respectively. More detail of processes, such as the influence of O_2 and NO_3 on the fate and transport of SO_4-S, nitrification, and microbially-mediated chemical reduction of O_2 and NO_3, are summarized in Bailey et al. (2013a) and Bailey et al. (2015).

3.2. Salinity equilibrium chemistry module for UZF-RT3D

The SEC module predicts major ion solute chemistry in a variably-saturated groundwater system. The chemical system considered in the SEC module is presented in Table 3 and includes eight aqueous components, ten complexed species, five solid species, and four exchange species. These components are selected due to their presence in the majority of soil-aquifer systems. Additional components can be included if needed for a particular study site. The module includes the major physical-chemical processes for salt ions: precipitation-dissolution of salt solids, aqueous complexation, and cation exchange. As these processes are contained in numerous other water quality models, only the basic procedure of implementation algorithms is discussed here, with full equations provided in Supplementary Material.

Table 3
Groups of species considered in the SEC module for UZF-RT3D/SEC.

Group	Species
Solid species	$CaSO_4$, $CaCO_3$, $MgCO_3$, NaCl, $MgSO_4$
Complexed species	$CaSO_4^0$, $MgSO_4^0$, $CaCO_3^0$, $CaHCO_3^+$, $MgCO_3^0$, $MgHCO_3^+$, $NaSO_4^-$, KSO_4^-, $NaHCO_3^0$, $NaCO_3^0$
Exchanged species	Ca, Mg, Na, K
Aqueous species	Ca^{2+}, Mg^{2+}, Na^+, K^+, SO_4^{-2}, CO_3^{2-}, HCO_3^-, Cl^-

3.2.1. Solution chemistry algorithm

Similar to other models such as PHREEQC (Parkhust and Appelo, 2013) and MINTEQA2 (Allison and Kevin, 1991; Paz-Garcia et al., 2013), the concentration of ions at equilibrium is determined using the stoichiometric approach of solving both mass balance and mass action equations simultaneously. The approach incorporates the Newton-Raphson method for solving the non-linear systems of equations. The law of mass action determines the concentration of each ion, with the concentration of reactants and products relates using an equilibrium constant K:

$$a\ \mathrm{A} + b\ \mathrm{B} \rightarrow c\ \mathrm{C} + d\mathrm{D} \tag{4}$$

$$K = \frac{(\mathrm{C})^c(\mathrm{D})^d}{(\mathrm{A})^a(\mathrm{B})^b} \tag{5}$$

where A, B, C, and D represent reactants and a, b, c, and d are constants, and where parentheses denote solute activities. Every possible reaction for the component species listed in Table 3 must be written in the form of Eq. (4). Following standard procedure, the activity coefficient is calculated using the ionic strength within either the Debye-Huckle or Davis equations (described in Supplementary Material). Mass balance equations are written for each ion, e.g. for SO_4:

$$SO_{4_T} = [SO_4^{2-}] + [CaSO_4^0] + [MgSO_4^0] + [NaSO_4^-] + [KSO_4^-] \tag{6}$$

where T denotes the total concentration of the aqueous component and brackets indicate the molality of the species within the solution. The total concentration of each species in the solution is the summation of free ions and the complexed forms of that ion. Salt ion mass is assumed to be subject to complexation, cation exchange, and precipitation-dissolution:

Complexation: The presence of aqueous complexes increases the solubility of minerals since complexation lowers the activity of the free ion (Appelo and Postma, 2005). The ten considered complexed species are shown in Table 3. Based on the law of mass action, the equilibrium constants are defined for the complexed species $CaSO_4^0$ and $CaCO_3^0$ as:

$$K_1 = \frac{(Ca^{2+})(SO_4^{2-})}{(CaSO_4^0)} \tag{7}$$

$$K_2 = \frac{(Ca^{2+})(CO_3^{2-})}{(CaCO_3^0)} \tag{8}$$

The equilibrium constants for the remaining eight complexed species are defined in the Supplementary Material, and values for all ten equilibrium constants are listed in Table 4.

Cation exchange: UZF-RT3D (Bailey et al., 2013a) simulates sorption onto soil particles using the linear, Freundlich, or Langmuir sorption

Table 4
Equilibrium constant values for complexed species (From Truesdell and Jones, 1974).

Equilibrium constant	Value [dimensionless]
K_1	0.004866
K_2	0.000599
K_3	0.078584
K_4	0.004699
K_5	0.001324
K_6	0.130586
K_7	0.12
K_8	0.054
K_9	0.562
K_{10}	0.1413

Table 5
Selectivity coefficient values for cation exchange reactions (From Robinns et al., 1980).

Gapon selectivity coefficient	Value [dimensionless]
K_{s1}	0.7
K_{s2}	6
K_{s3}	0.4
K_{s4}	0.2
K_{s5}	4
K_{s6}	16

isotherms. However, the use of isotherms ignores the electrostatic effects of the charges. Cation exchange replace-ability must be calculated considering electrostatic forces to determine the adsorbed ion to the soil particles and the released ion from particles to the solution, with the order of replace-ability determined by Coulomb's law and found to be Na > K > Mg > Ca. The Gapon equation is used to simulate exchangeable amount (see Supplementary Material) and Values of the associated selectivity coefficients are listed in Table 5.

Precipitation-dissolution: This process accounts for the dissolution and precipitation of solid salt minerals such as $CaSO_4$. The stoichiometric reaction for a salt solid AB_s and the free ions A^+_{aq} and B^-_{aq} is:

$$AB_s \leftrightarrow A^+_{aq} + B^-_{aq} \quad (9)$$

If the solution is super-saturated then the concentration of A^+_{aq} and B^-_{aq} will decrease as AB_s precipitates out of solution. On the other hand, if the solution is under-saturated the concentration of the species will increase as AB_s dissolves into A^+_{aq} and B^-_{aq}. Salt solids included in the present SEC module are $CaSO_4$, $CaCO_3$, $MgCO_3$, $MgSO_4$, and NaCl since they are common in many groundwater environments (see Table 3). Each mineral and accompanying reaction has a solubility product (Table 6). For the SEC module, solids are added to the system one at a time: the solid with lower solubility precipitates first, and the direction of each reaction (precipitation or dissolution) is determined comparing the solubility limits of each specific solid.

3.2.2. Verification of the SEC module

Before applying the coupled model to the regional-scale study (Section 4), the SEC module was tested for accuracy by comparing

Table 6
Solubility product values for salt solids used in the model application (From Haynes et al., 2016).

Salt mineral name	Solubility product	Value [dimensionless]
$CaSO_4$	K_{sp1}	4.9351×10^{-5}
$CaCO_3$	K_{sp2}	3.0702×10^{-9}
$MgCO_3$	K_{sp3}	4.7937×10^{-6}
$MgSO_4$	K_{sp4}	7.2440×10^{-3}
NaCl	K_{sp5}	37.3

Table 7
Comparison between the developed SEC module with Lucia et al. (2015).

Ion	Initial Concentration (mol/L)	Concentration at equilibrium (Lucia et al., 2015) (mol/L)	Concentration at equilibrium (This study: SEC module) (mol/L)
Ca^{2+}	1.8125×10^{-2}	1.40182×10^{-6}	1.40130×10^{-6}
Mg^{2+}	1.8125×10^{-2}	2.18876×10^{-3}	2.18855×10^{-3}
CO_3^{2-}	3.6251×10^{-2}	2.19016×10^{-3}	2.19035×10^{-3}

model results with data presented by Lucia et al. (2015) in a study of C sequestration that used a new algorithm for determining the equilibrium solubility limits over Newton's method. The system considers a mixture of CO_3, Ca, and Mg with 0.0362, 0.0181, and 0.0362 molalities, respectively, which is representative of ion concentrations in most of the reservoirs in their study region, with the ion concentrations suggesting the precipitation of Ca or Mg salts. The result of this comparison is shown in Table 7, with a maximum difference between the two models of 0.04%.

3.2.3. Implementing the SEC module in UZF-RT3D

The SEC module is written in FORTRAN for ease of linking with UZF-RT3D and is divided into three sub-modules, one each for precipitation-dissolution, aqueous complexation, and cation exchange with internal iteration criteria and an additional global criteria. Although most of these reactions are time-dependent but fast, it is assumed that the reactions have time enough to reach equilibrium. Aqueous reversible reactions have high kinetic rates which makes the mentioned assumption legitimate (Paz-Garcia et al., 2013). The solution strategy and calculation steps are summarized in Fig. 2. First, the concentration of each ion is provided to the Precipitation-Dissolution sub-module starting with the salt mineral that potentially precipitates first. The Precipitation-Dissolution sub-module continues until the internal criteria is satisfied, which is set to 0.01% for salt ion concentrations before and after precipitation-dissolution reactions occur for all possible salt solids. Once the new equilibrium concentration has been determined by the Precipitation-Dissolution sub-module, the Complexation sub-module is run and the concentration of free ions and complexed species is calculated. The updated concentrations of the ions then are provided to the Cation Exchange sub-module, which updates the concentrations. Calculations within each sub-module are repeated until the criterion for ionic strength is fulfilled.

The flow of data and calculations in the Precipitation-Dissolution sub-module are shown in Fig. 3 with the five solids considered successively. To determine the direction of reaction (precipitation or dissolution), the saturation index (Q_{sp}), equal to the product of the ion pair concentrations, is calculated. If Q_{sp} is equal to K_{sp}, the solution is in equilibrium with respect to the solid and neither precipitation nor dissolution will take place. If Q_{sp} is less than K_{sp}, the solution is under-saturated with respect to the solid and dissolution will occur until Q_{sp} is equal to K_{sp}. If there is enough salt mineral mass available for saturation to be reached, then only a portion of the salt mineral will be dissolved, otherwise all of the present salt mineral will be dissolved. If Q_{sp} is greater than K_{sp}, the solution is over-saturated with respect to the solid and precipitation will occur until equilibrium has been reached.

The general governing equation (Eq. (1)) has two terms on the right-hand side. The first term includes the transport processes and the second term considers the reactions within the SEC module. Because of the second term, Eq. (1) is highly non-linear. Hence, coupling between the transport and chemical calculations of UZF-RT3D and the SEC module is performed using a sequential non-iterative approach (Walsh et al., 1984; Yeh and Tripathi, 1989; Barry et al., 2000; Schoups et al., 2006; Carrayrou et al., 2004), in which the transport and chemical kinetic equations of UZF-RT3D are followed by internal iterations for equilibrium chemical reactions. The calculation steps of the coupled

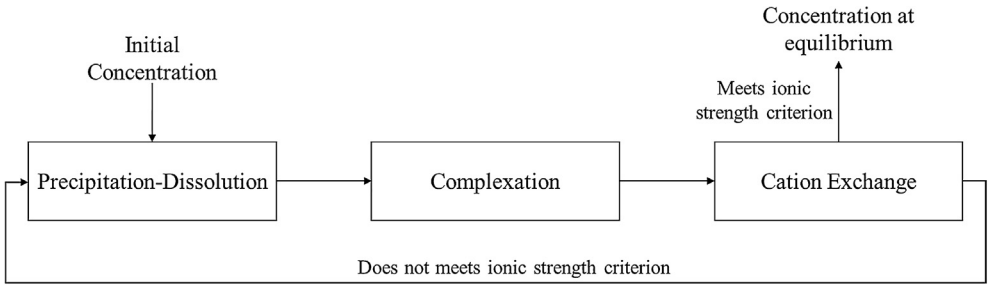

Fig. 2. Information flow within the Salinity Equilibrium Chemistry (SEC) module of UZF-RT3D.

model, with inputs from MODFLOW-NWT, are shown in Fig. 4.

For each time step, UZF-RT3D first solves for concentration of each solute at each finite-difference grid cell according to advection, dispersion, source/sink mixing (solutes entering/leaving the aquifer via groundwater sources/sinks), and kinetic reactions, with the latter including the cycling of C, N, and S. Concentrations for each ion at each grid cell are then provided to the SEC module, with ion concentrations updated using the methods described in the previous section. The fifth and sixth terms on the right-hand side of Eq. (2a) are equal to zero for the species that are not included in the SEC module. The updated concentrations are then provided for the start of the next time step, with this coupling proceeding until the end of the simulation. In this coupling, the local equilibrium concept is adopted, in which the duration of the selected time step is assumed long enough for all interactions between chemical constituents to reach equilibrium (Rubin, 1983; Javadi and Al-Najjar, 2007; Al-Hamdan and Reddy, 2008).

4. Model application at the regional scale

4.1. Study Region: Lower Arkansas River Valley, Colorado, USA

The UZF-RT3D/SEC model was applied to a 500 km^2 stream-aquifer system within the Lower Arkansas River Valley (LARV) in southeastern Colorado (Fig. 5). For more than 130 years the region has been one of the most productive agricultural areas in Colorado. Crops include alfalfa, melons, corn, beans, sorghum, wheat, grass, and vegetables. The climate is semi-arid, with average monthly rainfall ranging from 0.7 cm during the period October-March to 5.0 cm during the period April–-September. Irrigation is practiced from March to November, with irrigation water diverted from the Arkansas River via six irrigation canals or 575 pumping wells (see Fig. 5 for locations) from the alluvial aquifer due to the low rainfall in the region. Within the upstream study region, there are eight tributary drainages, and three surface storage reservoirs allocating water on the basis of prior appropriation water rights.

The region is impaired by high salinity in groundwater, surface water, and soil, caused by the existence of salt minerals, particularly gypsum ($CaSO_4$), waterlogging in the shallow subsurface (Konikow and

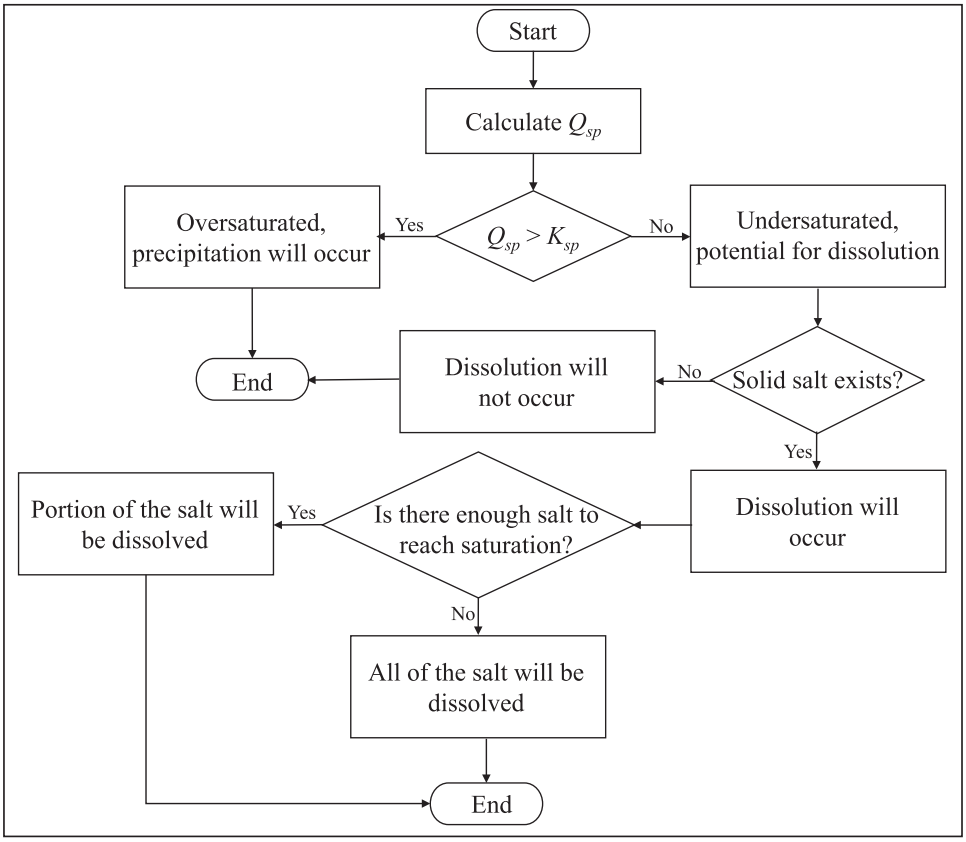

Fig. 3. Flow chart for the precipitation-dissolution sub-section of the Salinity Equilibrium Chemistry (SEC) module of UZF-RT3D.

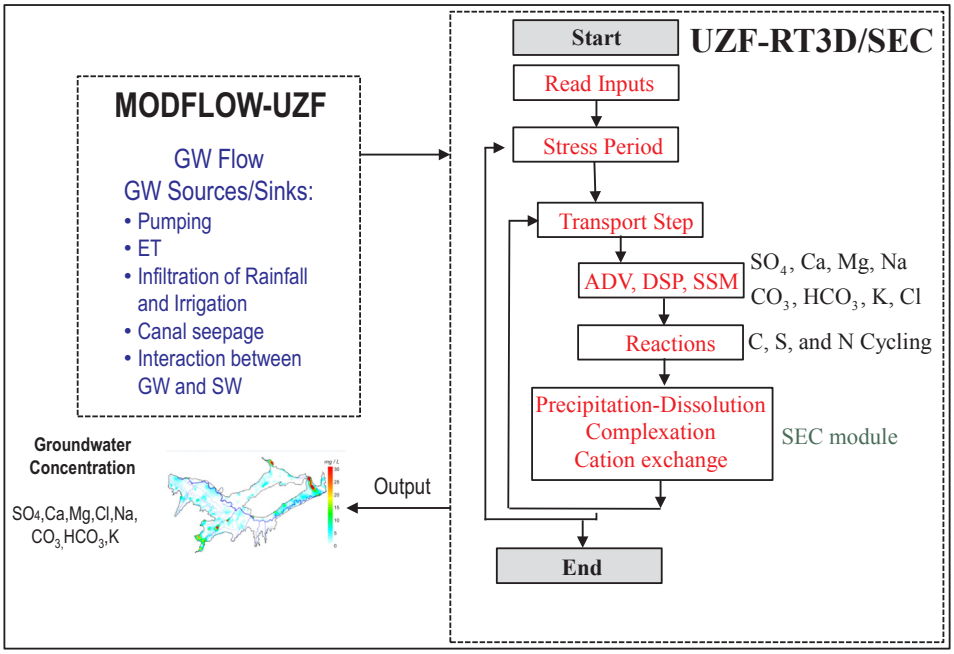

Fig. 4. UZF-RT3D model code flow chart, showing the input from MODFLOW-UZF and the inclusion of the SEC module during the transport time step.

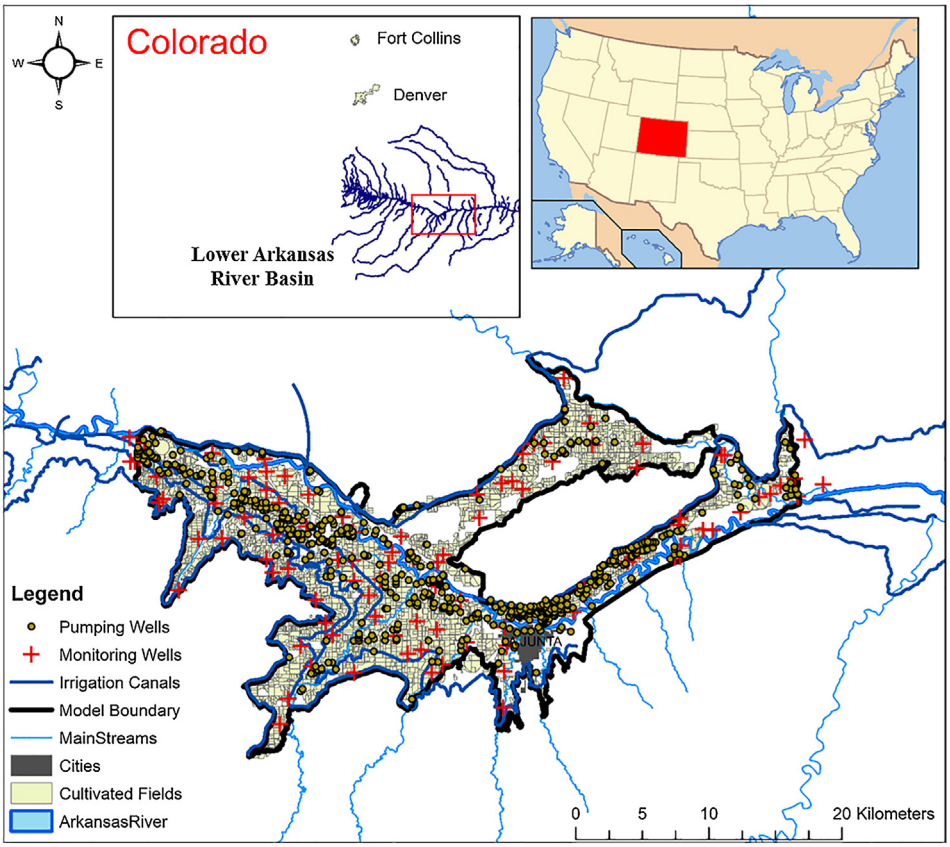

Fig. 5. Location of the model study region, showing the Arkansas River and its tributaries, irrigation canals, cultivated fields, monitoring wells, and pumping wells.

Person, 1985; Hukkinen, 1993; Goff et al., 1998; Morway and Gates, 2012; Gates et al., 2002, 2016), and evaporative concentration. Fig. 6 shows salt ion proportions from the analysis of 389 groundwater samples in the study region using a Piper Diagram (Piper, 1944), illustrating the hydro-geochemical facies of samples. The samples were collected between 2006 and 2009 from the monitoring wells shown in Fig. 5. Results indicate that the majority of the samples are type Ca-SO_4, due to the dominant presence of gypsum. Frequency histograms of C_{TDS}, $C_{SO4\text{-}S}$, and C_{Ca} in groundwater samples are shown in Fig. 7A–C respectively. Comparing the spatio-temporal average C_{TDS} in the groundwater (2732 mg/L) with the estimated maximum permissible C_{TDS} value for irrigation without crop yield reduction (~700 mg/L) (Ayers and Westcot, 1985) indicates the severity of salinization in the region. Also, the secondary EPA drinking water standard for C_{SO4} is

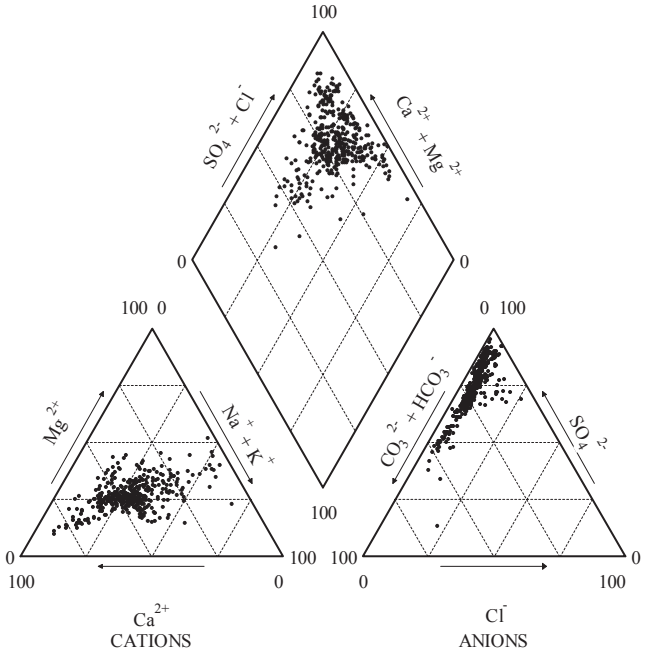

Fig. 6. Piper diagram of salt ion concentrations in groundwater samples from the study region over the modeled period. Units are normalized and expressed as a percent of proportional mass per cation/anion. Results demonstrate that SO_4 and Ca are the dominant anion and cation, respectively.

250 mg/L, much less than the observed average of 630 mg/L (for $C_{SO4\text{-}S}$) in the study region. Previous studies have estimated average crop yield reduction of up to 7% in the region due to high salinity in the soil root zone (Gates et al., 2002; Morway and Gates, 2012).

The groundwater flow patterns in the study region have been simulated by Morway et al. (2013), who used MODFLOW with the UZF package for unsaturated zone flow (Niswonger et al., 2006). The region is discretized into 250 m by 250 m grid cells horizontally and three layers vertically from ground surface to the shale bedrock (average depth is 15 m). The model accounts for infiltrated rainwater and irrigation water, which result in deep percolation that recharges the unconfined aquifer. Seepage from irrigation canals and reservoirs, along with occasional seepage from the Arkansas River and its tributaries, are other key components of subsurface influx. Groundwater pumping from wells, upflux from the shallow water table, ET from cropped and naturally-vegetated areas, and discharge to the Arkansas River and its tributaries are key components of subsurface discharge (Morway et al., 2013). The model was run for the period 1999–2007, which was extended in a later study through 2009 (Bailey et al., 2014). As example model input and output, the calibrated cell-by-cell values of hydraulic conductivity (m/d) are shown in Fig. 8A, and the cell-by-cell average depth to water table during the simulation period is shown in Fig. 8B.

The UZF-RT3D/SEC model uses the flow patterns and sources/sinks from the MODFLOW model, with the same areal discretization but with six vertical layers spanning the depth between the ground surface and the shale bedrock. The top two layers are each 0.5 m in thickness to simulate solute chemistry and C, N, and S cycling in the root zone. The third layer is 1.0 m, and the thickness of the remaining three layers is divided evenly over the remaining depth to the shale bedrock. Shultz et al (2018) previously calibrated the UZF-RT3D component of the model in the region for redox reactions involving O_2, NO_3, and selenium, and Tavakoli Kivi and Bailey (2017) calibrated it for S cycling. The model is run from January 1, 2006 to October 31, 2009 using daily time steps.

Concentration of the major ions in both surface water irrigation and groundwater irrigation is accounted for. For surface irrigation, with water derived from adjacent irrigation canals, the concentrations are

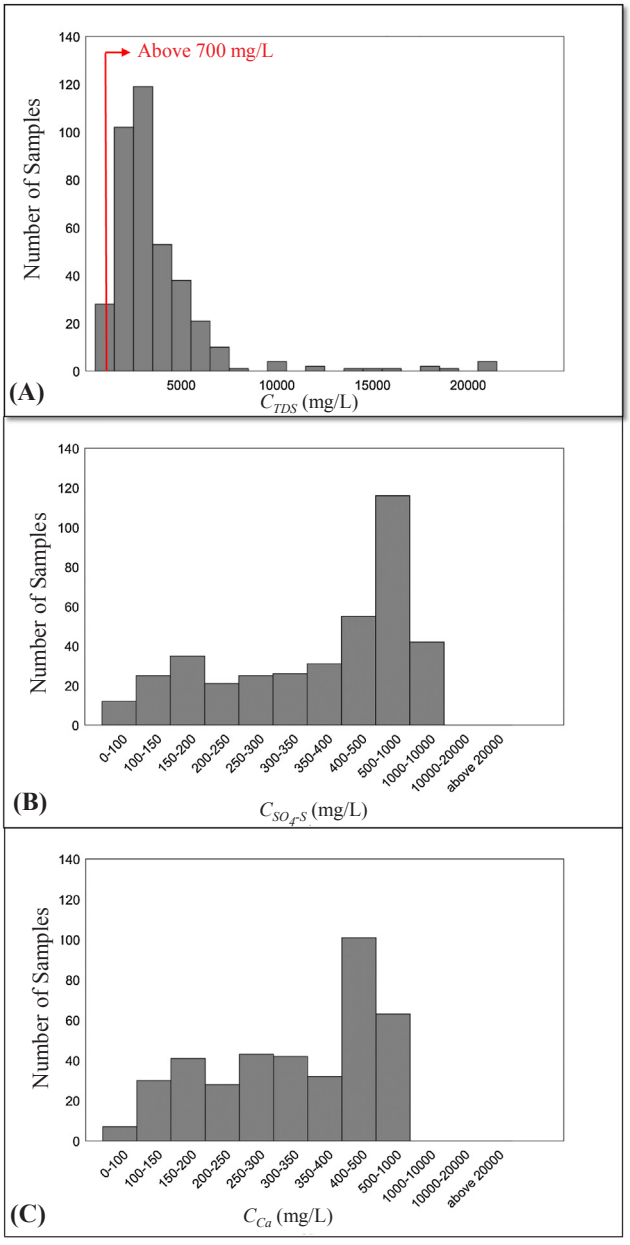

Fig. 7. Histogram of (A) C_{TDS}, (B)C_{SO_4-S}, and (C) C_{Ca} in groundwater samples in the study region.

specified using results from the analysis of canal water samples which were taken periodically in the river near the canal diversion during the simulation period (see Table S2 in Supplementary Material for concentration values). For groundwater irrigation, concentration values of the ions are simulated by UZF-RT3D/SEC at the location of the well screen (layer 4 of the model). For areas where water from canals, tributaries, and the Arkansas River seeps into the aquifer, the salt ion concentrations in the surface water are estimated from field samples collected during the simulation period (see Table S2 in Supplementary Material for values).

Crop parameters are provided for each crop type in the LARV study region (see Fig. 9 for spatial distribution of crop type in 2006). These parameters govern the management and growth of each crop, and include the typical planting, harvesting, and plowing dates; fertilizer application and uptake; root growth and death; and C/N and C/S ratios. Parameters for organic matter decomposition, oxidation-reduction reactions, crop uptake, and linear sorption also are provided for C, N, and

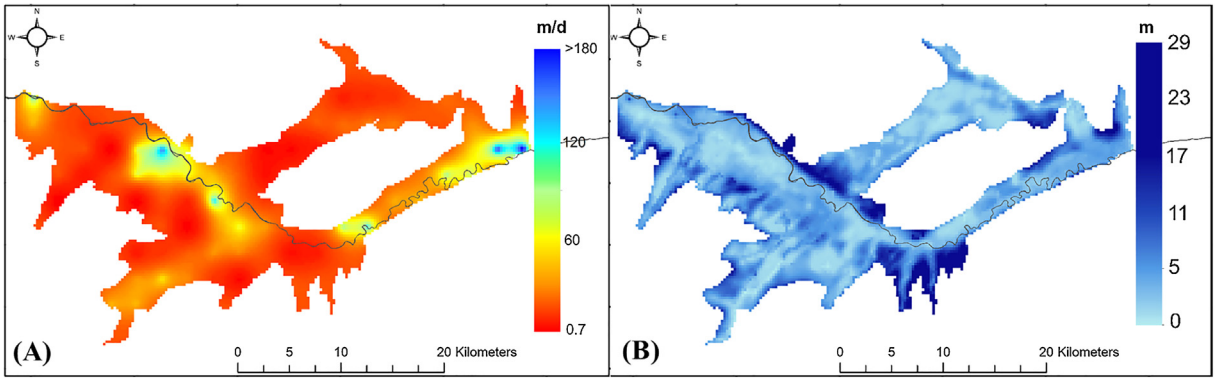

Fig. 8. (A) Hydraulic conductivity (m/d) of the upper alluvium material, based on a tested groundwater flow model of the region (Morway et al., 2013), and (B) Average depth to the water table (m), as simulated by the flow model.

S cycling and for the chemical reduction of O_2, NO_3, and SO_4 in groundwater. These values are the same as those used in the S cycling and SO_4 transport model of Tavakoli Kivi and Bailey (2017), and are included in Supplementary Material (Tables S3 and S4).

Parameters used in the SEC module are the same as those described in Section 3 (see Tables 3–7). The initial spatial distribution of salt minerals, $CaSO_4$ and $CaCO_3$, which is mapped to the individual grid cells, is based on a soil survey performed by the USDA's Natural Resources Conservation Service (NRCS) (https://websoilsurvey.sc.egov.usda.gov/App/WebSoilSurvey.aspx). Data for $CaSO_4$ and $CaCO_3$ are expressed as a percent by weight, with values up to 45% and 8%, respectively, for the minerals.

4.2. Model calibration and testing

4.2.1. Comparing model results with field data

Estimation of model parameters in the coupled model involved analyzing solute concentrations and groundwater salt ion mass loadings during a spin-up simulation and during the 2006–2008 calibration period, with field data from 2008 to 2009 used as testing data. The spin-up simulation was included to achieve steady seasonal fluctuations of salt ion concentration in the aquifer and a steady fluctuation of groundwater salt ion mass loading to the Arkansas River, and was prepared by repeating the cropping and flow pattern for the year 2006 for 10 years using crop and chemical reaction parameters from Bailey et al. (2014).

The comparison of model results with measured values during the calibration and testing periods was conducted in a manner advocated by Konikow (2011), with the objective of reproducing major trends and spatio-temporal statistics rather than time series of concentrations at point locations of measurement (e.g. monitoring wells), the scale of a model grid cell being 10^7–10^8 times larger than that of a measurement location within the cell. With this objective, model results were tested against observed spatio-temporal averages of concentration for each salt ion, with spatial averages occurring by irrigation command area (Fig. 10) due to the unique water rights priority, irrigation, and cultivation histories of each command area. Results also are compared using the frequency distribution of concentration for each salt ion. These comparisons are performed for each salt ion in the saturated zone of the aquifer.

For the soil root zone, the frequency distribution of C_{TDS} is compared between the model and values derived from more than 54,000 electromagnetic induction measurements in relation to saturated paste soil electrical conductivity (EC_e) in many fields scattered across the study region (Morway and Gates 2012). The estimated EC_e values (dS/m) are converted to C_{TDS} (mg/L) using a relationship that exists between EC_e and C_{TDS} in groundwater samples collected in the saturated zone (Gates et al., 2016). For the model, C_{TDS} for each grid cell in the

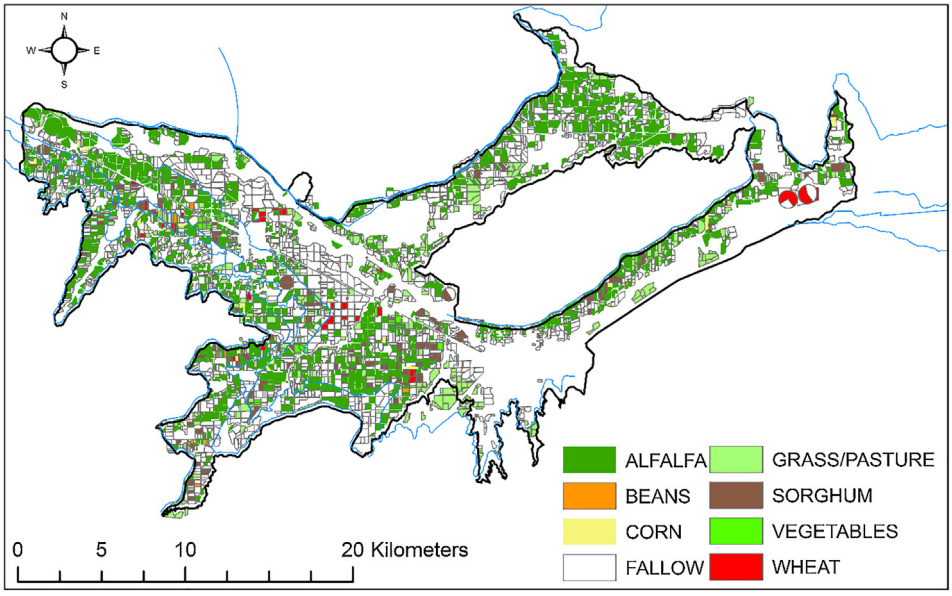

Fig. 9. Crop type of each cultivated field in the study region during the 2006 growing season.

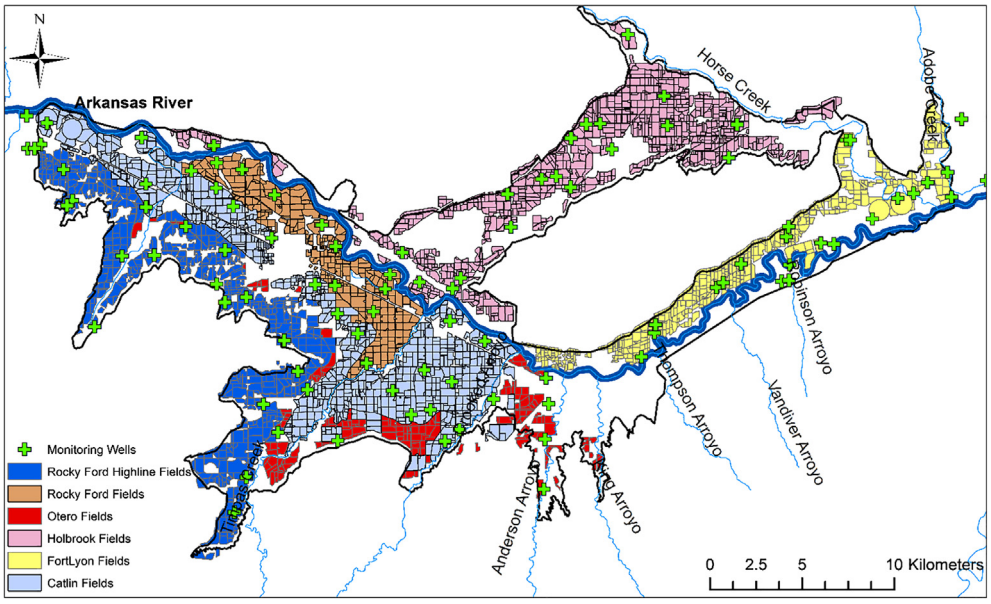

Fig. 10. Map of the study region showing the location of groundwater monitoring wells and the canal command areas (i.e. the sets of cultivated fields receiving irrigation water from each canal).

top 2 layers of the model is computed by summing the simulated concentrations of the ions. Since the EC_e values were estimated using saturated paste extracts from field soil samples, only model results from cells with a near-saturation water content (above 95%) were included in the frequency distribution comparison.

In addition to using groundwater solute concentrations for model testing, stochastic river mass-balance calculations for the stream system (Gates et al., 2018) were used to determine the approximate daily mass loadings of SO_4 and TDS to the Arkansas River that are not accounted for by measured loading from the tributaries. It is assumed that a substantial portion of the unaccounted-for mass loading, especially during the non-irrigation season, can be attributed to mass loading from the aquifer to the Arkansas River, and thereby provides an additional test for model results.

4.2.2. Parameter estimation methodology

Estimation of parameters in the SEC module was performed using a joint manual and automated calibration approach to achieve a satisfactory match between observed and simulated target variables. Target variables include spatially-averaged $C_{SO4\text{-}S}$, C_{Ca}, C_{Mg}, C_{Na}, C_{Cl}, C_{HNO3} and C_{TDS} in the saturated zone; spatially-averaged C_{TDS} of soil water in the root zone; the relative frequency distribution of all major salt ions in the saturated zone; the relative frequency distribution of C_{TDS} in soil water in the root zone; and groundwater mass loading of SO_4 and TDS to the Arkansas River.

A variant of the Brier Score (BS) (Brier, 1950), which compares the relative frequency distribution of two sample sets and commonly is used to evaluate probability distribution performance, is computed in this study for a relative frequency histogram of n_b classes, or bins, as:

$$\mathrm{BS} = \left(\frac{1}{n_b}\right) \sum_{1}^{n_b} (F_i - O_i)^2 \tag{10}$$

where F_i is the relative frequency of simulated values in the i^{th} bin and O_i is the relative frequency of observed values in the i^{th} bin. The value of $\sqrt{\mathrm{BS}}$ ranges between 0 and 1, providing a measure here of the average discrepancy between simulated and observed relative frequency, with values of $\sqrt{\mathrm{BS}}$ closer to 0 indicating a better match.

As part of the initial step of the calibration process, the solid salt contents in the soil profile and in the aquifer were manually adjusted within the range of values reported in the NRCS soil survey data to yield simulated C_{TDS} values in the soil root zone and aquifer that were similar to the observed soil and aquifer data. Preliminary simulations also indicated that model results are strongly dependent on the solubility product K_{sp} for each salt represented in the model, which are governed by temperature and pH. Since the temperature in the root zone and in the deep layers of the aquifer differs seasonally, a value of K_{sp} was assigned to each of the saturated and unsaturated zones for each salt mineral. Once the salt distribution was determined, the PEST (Parameter Estimation) software (Doherty, 2007) was used to refine the solubility products of each salt solid. PEST adjusts selected parameters in sequential simulation runs to minimize the objective function, which is the sum of the squared weighted residuals between the observed and simulated values:

$$\Phi = \sum_{i}^{n_v} w_i \left(O_{v_i} - M_{v_i}\right)^2 \tag{11}$$

where Φ is the objective function, n_v is the number of target variables, w_i is the weight assigned to the ith target variable, and O_{v_i} and M_{v_i} are the observed and simulated values of the i^{th} target variable, respectively. The value of w_i for each target variable is calculated as the product of an uncertainty weight and a unit discrepancy weight. The uncertainty weight, was calculated as the inverse of an estimated coefficient of variation (CV) reflective of the relative uncertainty in the observations of the target variable. The unit discrepancy weight, was determined by unifying the sum of the square of each observed variable value.

An iterative approach using both the spin-up simulation and the 2006–2008 simulation was used in the model calibration procedure due to the dependence of initial concentrations in 2006 on the long-term spin-up simulation. Initial K_{sp} values for the SEC module were assigned from the literature (Table 6). The overall procedure is as follows:

a. Establish a preliminary set of initial conditions for the 2006–2008 simulation using a 30 year spin-up simulation, which included manual adjustment of solid salt contents in the soil and aquifer to achieve reasonable similarity between simulated and observed C_{TDS} values;
b. Use PEST to provide an estimate of K_{sp} values according to command area;
c. Re-run the spin-up simulation with the new set of K_{sp} values to

Table 8
Calibrated solubility product for salt solids using PEST.

Solubility product	Unsaturated zone	Saturated zone	Range	References
K_{sp1}	4.9300×10^{-5}	3.5691×10^{-5}	1.32×10^{-5}–6.89×10^{-5}	1
K_{sp2}	3.0700×10^{-9}	3.7037×10^{-9}	5.41×10^{-10}–4.15×10^{-9}	2
K_{sp3}	4.7900×10^{-6}	4.7937×10^{-6}	2.38×10^{-6}–6.82×10^{-6}	3
K_{sp4}	0.0070	0.0071	0.006–0.049	4
K_{sp5}	37	37.2	36.77–41.73	5

1 – Krumgalz (2017) and Merkel and Planer-Friedrich (2005).
2 – Lucia et al. (2015), Panthi (2003), Plummer and Busenberg (1982).
3 – Haynes (2016), Lucia et al. (2015), Case et al. (2011).
4 – Krumgalz (2017), Millero (2001), Pillay et al. (2005).
5 – Haynes (2016) and Zeng and Li (2015).

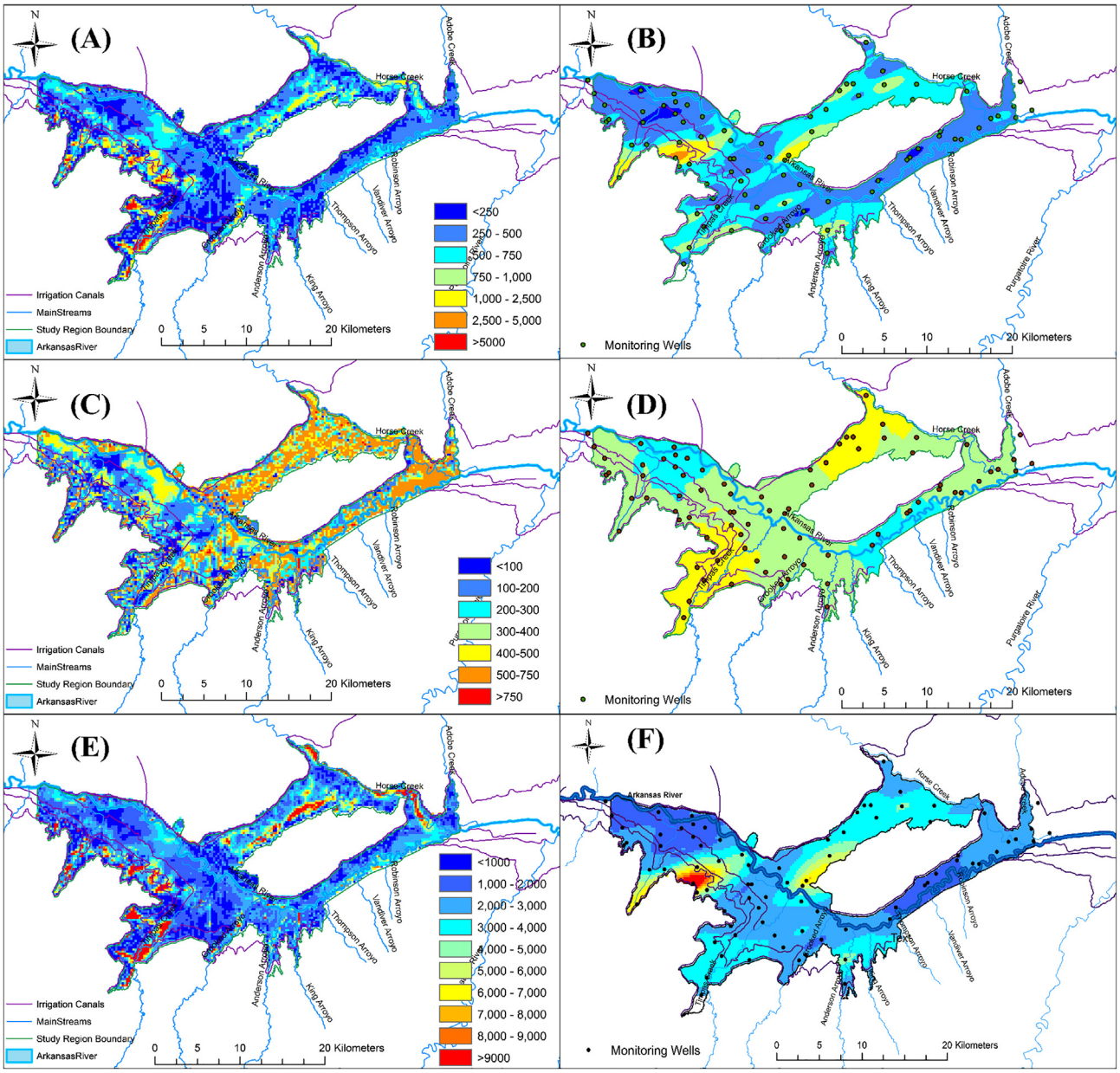

Fig. 11. Spatial raster plots of (A) average simulated C_{SO4-S} (mg/L), (B) average observed C_{SO4-S} (mg/L), (C) average simulated C_{Ca} (mg/L), (D) average observed C_{Ca} (mg/L), (E) average simulated C_{TDS} (mg/L), and (F) average observed C_{TDS} (mg/L) in the middle alluvium (layer 4 of the model) of the study region over the 2006–2009 simulation period.

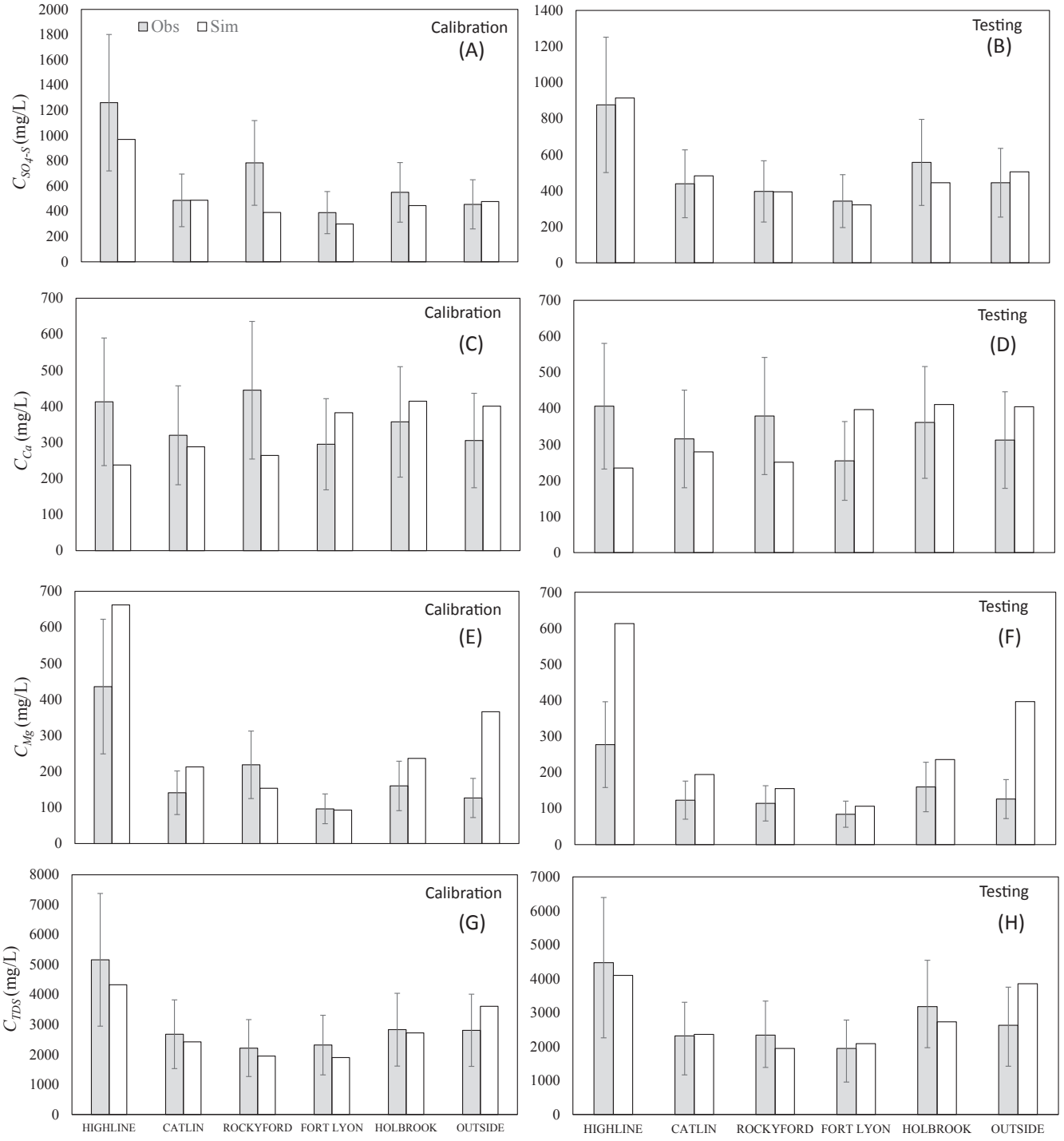

Fig. 12. Comparison of simulated and observed average C_{SO_4-S}, C_{Ca}, C_{Mg}, and C_{TDS} for each canal command area for the calibration period (A, C, E, G) and for the testing period (B, D, F, H).

establish new initial conditions, with comparisons made to estimated SO_4 and TDS mass loading to the Arkansas River. The spin-up simulation was re-run using K_{sp} values until the groundwater salinity mass loadings at the end of the spin-up simulation matched well with the range of observed daily groundwater salinity mass loadings during the 2006–2008 period;

d. A further adjustment was made comparing the model results to observed values within the test period by manually adjusting the K_{sp} values to achieve the best match between simulated and observed salt ion concentrations in the saturated zone.

Values of K_{sp} were assigned to each canal command area for both the soil root zone and the saturated zone and were estimated using PEST considering the target values. Parameter values resulting from the UZF-RT3D/SEC calibration process are shown in Table 8, all of which fall within the range of values reported in the literature.

4.3. Calibration and testing results

Fig. 11(A)–(E) show the cell-by-cell computed $C_{SO4\text{-}S}$, C_{Ca}, and C_{TDS} values in groundwater, averaged over the 2006–2009 simulation period. High levels of $C_{SO4\text{-}S}$ and C_{TDS} occur principally in the Rocky

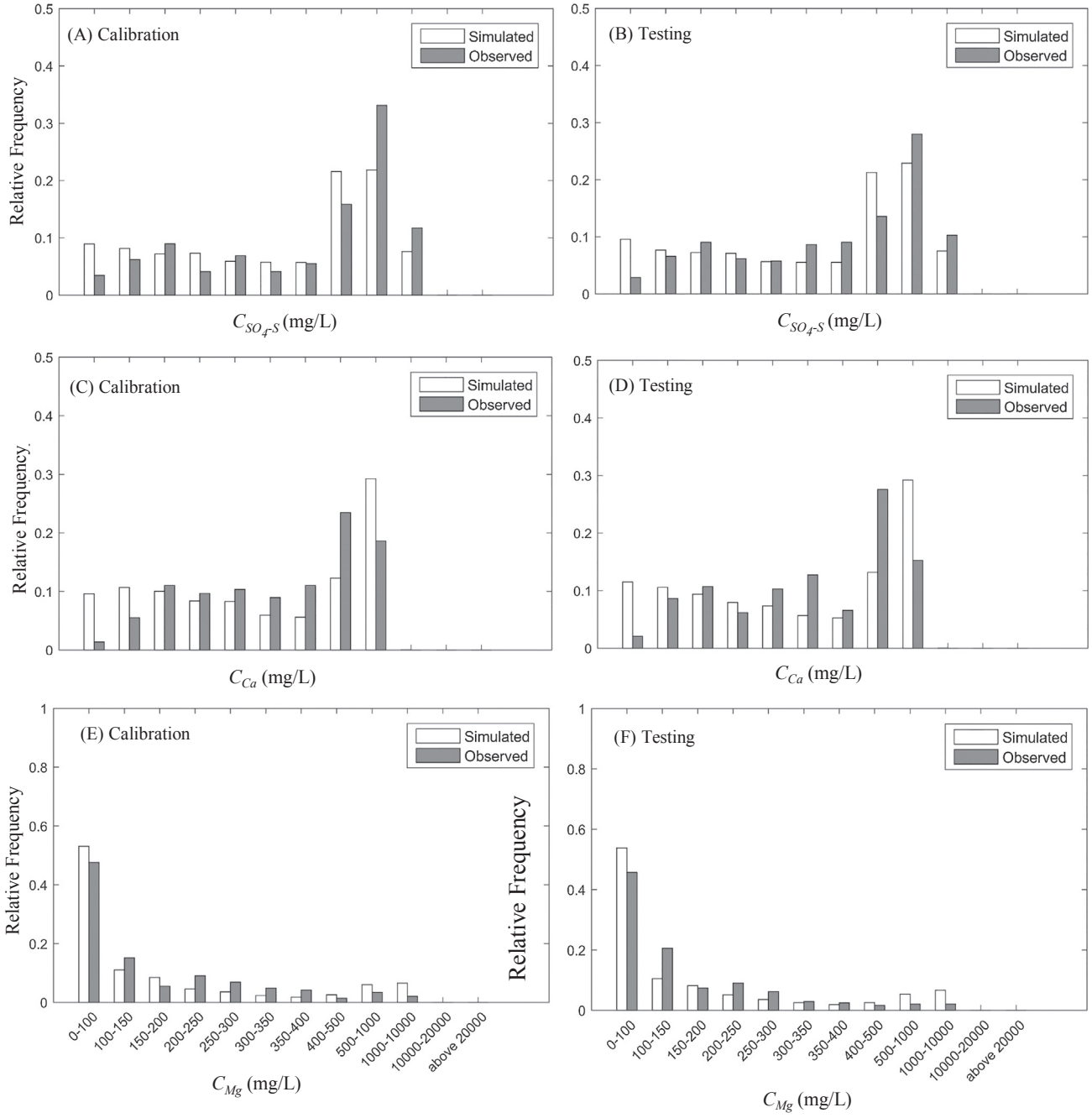

Fig. 13. Comparison of relative frequency histograms for simulated and observed C_{SO_4-S}, C_{Ca}, and C_{Mg} for the calibration period (A, C, E) and the testing period (B, D, F).

Ford Highline canal command area and in the Holbrook canal command area (see Fig. 10). Typically, areas of high C_{Ca} coincide with areas of high $C_{SO4\text{-}S}$ indicative of the presence of gypsum. The areas of highest concentration often are far from the Arkansas River, indicating that mass loadings of TDS to the river are lower than what could be expected if the plumes of high-concentration groundwater move towards the river over the coming years. Fig. 11(B), (D), and (F) shows a spatial comparison between the simulated and observed $C_{SO4\text{-}S}$, C_{Ca} and C_{TDS} values in groundwater averaged over the 2006–2009 period. The observed values for 2006–2009 period were averaged for each monitoring well and the Kriging method was used to construct contour plots based upon observed values. Kriging uses statistical interpolation to estimate concentrations at locations between observed values, while the calibrated MODFLOW-UZF and UZF-RT3D/SEC models use the governing flow and reactive transport equations. Thus, the methods are not directly comparable; nevertheless, model results demonstrate the capability of the model to reproduce overall observed spatial patterns of groundwater salinity. In particular, the zones of observed high salinity in the Rocky Ford Highline and Holbrook canal command areas have been captured by the model.

The comparison between the simulated and observed average values within each canal command area for $C_{SO4\text{-}S}$, C_{Ca}, C_{Mg}, and C_{TDS} in groundwater is shown in Fig. 12 for both the calibration and testing periods. Whiskers on the plotted observed values represent ± standard deviation of an assumed normal distribution with CV = 0.43, estimated following the method described in Bailey et al (2014) to account for uncertainty due to measurement error and scale discrepancy. Considering this uncertainty, model results are favorable compared to the

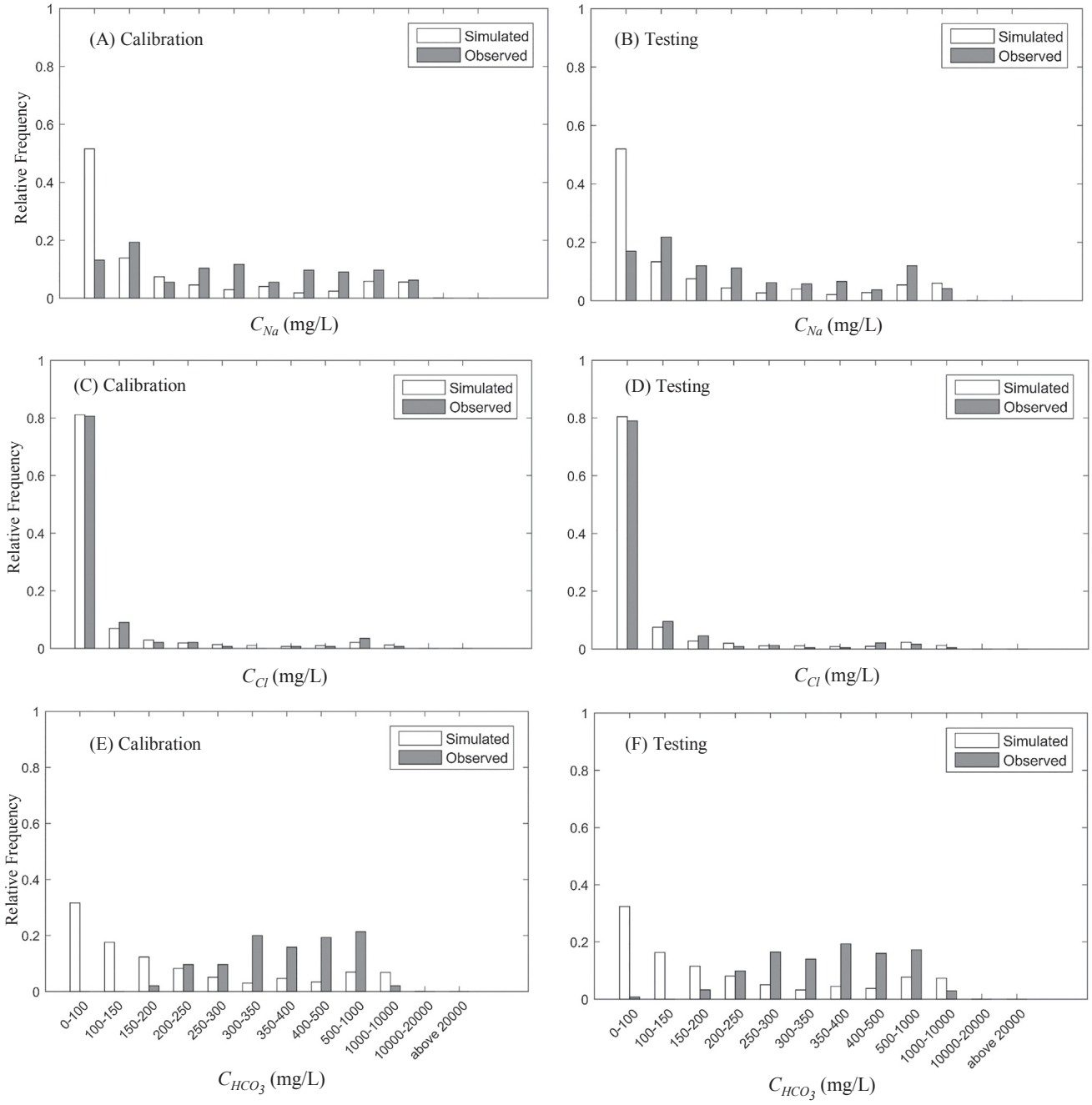

Fig. 14. Comparison of relative frequency histograms for simulated and observedC_{Na}, C_{Cl}, and C_{HCO_3} for the calibration period (A, C, E) and the testing period (B, D, F).

observed values. Interestingly, simulated and observed values for $C_{SO4\text{-}S}$ and C_{TDS} have a better match for the testing period than for the calibration period. The spatio-temporal average of simulated values of $C_{SO4\text{-}S}$ within a grid cells in layer 4 over the entire region is 512 mg/L for the calibration period and 510 mg/ L for the testing period, compared with respective average observed values of 655 mg/L and 509 mg/L. Layer 4 is chosen as the target layer since the groundwater monitoring wells typically are screened at a depth corresponding to the elevation represented by layer 4 in the model. For C_{TDS}, average simulated values in layer 4 are 2822 mg/L and 2845 mg/L for the calibration and testing periods, respectively, while average observed values are 3003 mg/L and 2813 mg/L for the calibration and testing periods.

Figs. 13 and 14 show relative frequency histograms for simulated values of $C_{SO4\text{-}S}$, C_{Ca}, C_{Mg}, C_{Na}, C_{Cl}, and C_{HCO3} in groundwater in layer 4 and for observed values. Although the previous comparison was made between the average values over the command region, these plots demonstrate the model's ability to reproduce the distributions of concentrations across the region and over the model calibration and testing periods. Eleven bins are used to create the relative frequency histograms, up to a value of 20,000 mg/L, with a twelfth bin representing values above 20,000 mg/L.

The values of $\sqrt{\text{BS}}$ for $C_{SO4\text{-}S}$, C_{Ca}, and C_{Mg} in groundwater for the calibration period are 0.04, 0.06, and 0.03, and for the testing period are 0.04, 0.07, and 0.04, respectively, indicating the model accurately replicates not only the averages of each concentration but also the frequency distributions of the observed data. The $\sqrt{\text{BS}}$ values for C_{Na}, C_{Cl}, and C_{HCO3} for the calibration period are 0.12, 0.01, and 0.14, respectively, and for the testing period are 0.11, 0.01, and 0.13.

The $\sqrt{\text{BS}}$ value for simulated C_{HCO3} and C_{Na} reveals poorer model

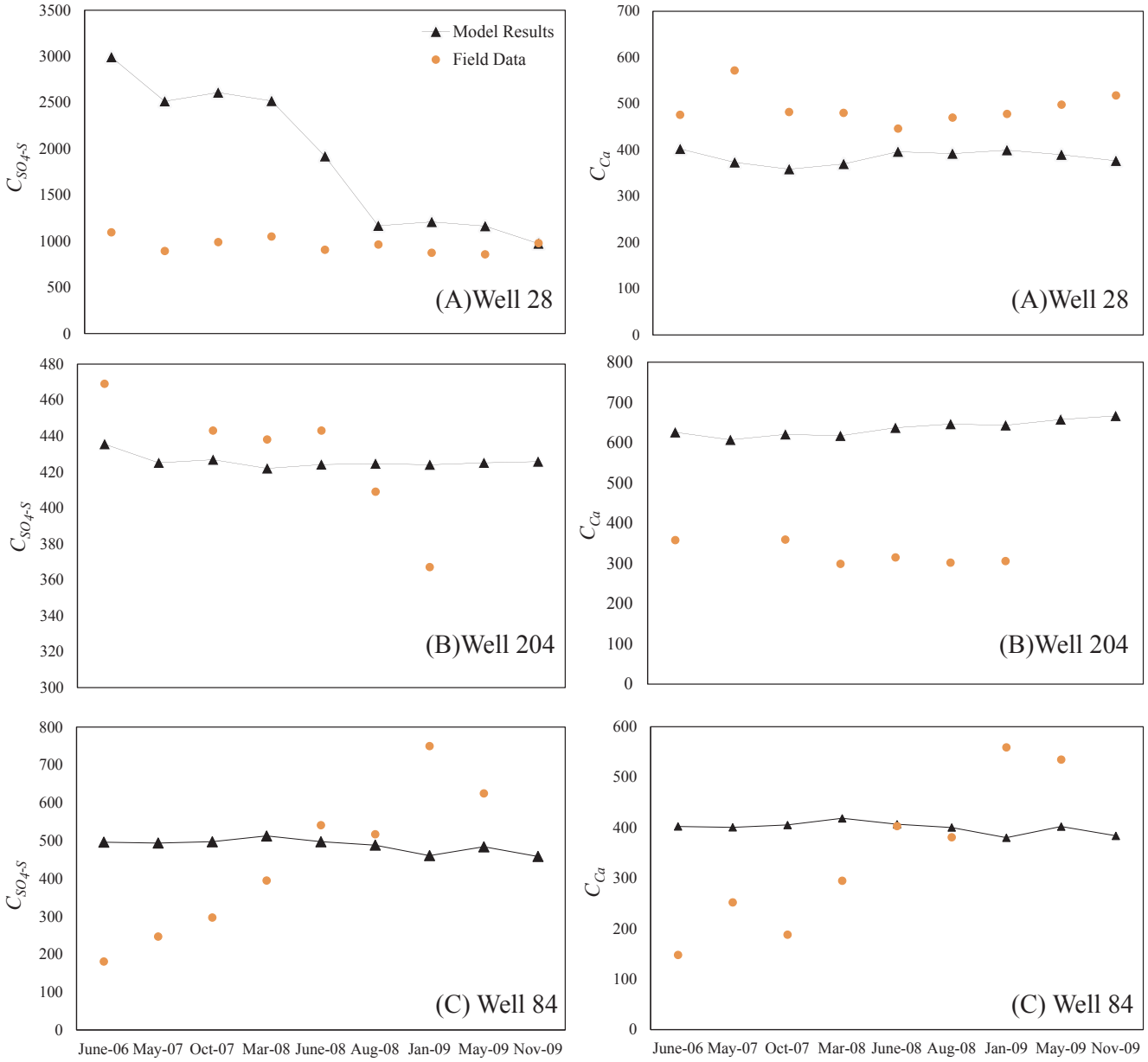

Fig. 15. Comparison of time-dependent C_{SO_4-S} and C_{Ca} measured in three monitoring wells (Well 28, Well 204, Well 84) and simulated values in the finite-difference grid cell that encloses each well, demonstrating a variety in model results with point measurements.

performance for these specific ions. The main source of HCO_3 in groundwater is the dissolution of $CaCO_3$, which is also a source of CO_3. The SEC module currently does not fully accommodate the C cycle in a closed system; instead, the simple dissolution formula for $CaCO_3$ in Eq. (34) is used (Millero, 2001). As a result, the model under-predicts C_{HCO3}. The main source of Na is dissolution of NaCl. In the LARV, as shown in Fig. 6, most of the groundwater samples are Ca-SO_4 type; thus, under-predicting C_{HCO3} and C_{Na} does not compromise the validity of this and similar applications in terms of total salinity transport and storage. By including the full C cycle and considering the partial CO_2 pressure, C_{HCO3} would be calculated as a secondary component in $CaCO_3$ dissolution.

Although not used in parameter estimation, time series of measured and simulated values of C_{SO4-S} and C_{Ca} are shown in Fig. 15 for three monitoring wells in the study region. Poor matches (see Well 204 for C_{Ca}) can result in these point-by-points comparisons, in part due to the large discrepancy between the model grid scale and the observation scale. Nevertheless, in general the model yields values of similar magnitude to the field data. If desired, cell-by-cell chemical reaction parameters could be calibrated, albeit with great computational effort and at the risk of over-fitting, to yield better matches with point measurements. However, the purpose of the model is to reproduce general spatial and temporal trends and distributions.

Fig. 16 shows the simulated cell-by-cell values of C_{TDS} in the root zone (top 1 m) soil water, averaged over the 2006–2009 simulation period. High soil salinity (> 10,000 mg/L) occurs in many areas in the region, principally in the fields irrigated by the Catlin and Rocky Ford Highline canals (see Fig. 10), and along Timpas Creek and Crooked Arroyo and certain reaches of the Arkansas River. The severity of the problem in regards to potential impact on crop yield is apparent when compared to permissible limits of C_{TDS} to avoid yield reduction for alfalfa and corn, the dominant crops in the LARV. Assuming an average soil water content at 40% of saturation in irrigated fields over the region, threshold C_{TDS} values of 4300 mg/L and 5100 mg/L can be estimated for corn and alfalfa, respectively (Grieve et al., 2012; Gates et al., 2016). The average value of C_{TDS} computed over the region and over

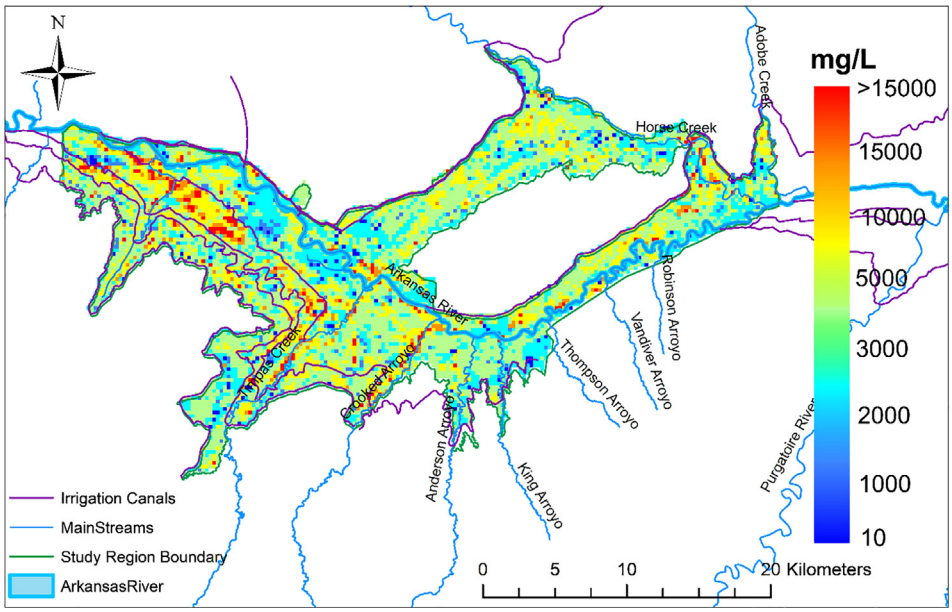

Fig. 16. Spatial raster plots of average simulated C_{TDS} (mg/L) in the root zone.

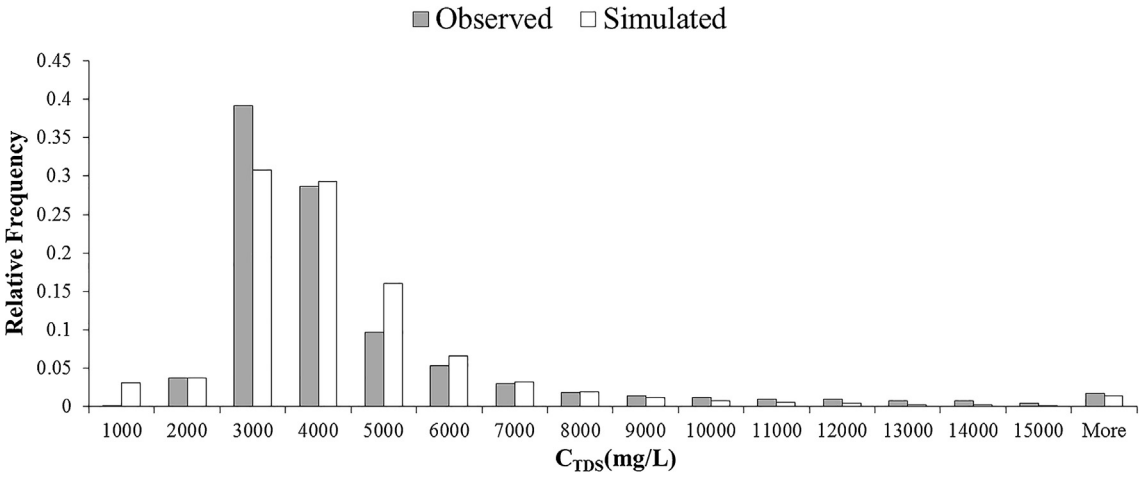

Fig. 17. Comparison of relative frequency of simulated and observed C_{TDS} in the soil root zone.

the simulation period was 4993 mg/L, suggesting that a substantial area is suffering from crop yield reduction. These results are comparable with the conclusions of Morway and Gates (2012) for this same region, with 22% of locations surveyed exceeding the crop-yield threshold. Also, higher C_{TDS} values are expected in areas with shallow groundwater where more salt enters the root zone by upflux from saline groundwater (Morway and Gates, 2012). Comparing the water table depth plot (Fig. 8B) with the location of high C_{TDS} in Fig. 16 complies with the same conclusion. The average value of simulated C_{TDS} for cells with near-saturated soil conditions (see Section 4.2.1) is 4034 mg/L, which matches favorably with the average observed C_{TDS} of 4180 mg/L in soil saturated extract samples. The relative frequency histograms of simulated and observed C_{TDS} values for near-saturated soil conditions are shown in Fig. 17. The value of $\sqrt{BS}$ is 0.03, indicating that the model can be employed to satisfactorily estimate soil salinity over a regional scale, allowing subsequent estimation of impacts on crop yields.

The simulated daily average SO_4 and TDS mass loadings from groundwater to the Arkansas River (kg/day) are shown in Fig. 18, with a comparison to statistics of the stochastic river mass balance estimates of total unaccounted-for mass loading. The model-predicted groundwater mass loading to the river typically is well within the stochastic mean minus one standard deviation and is below the stochastic mean. This is to be expected since the stochastic mass balance results include loading from unaccounted-for surface water returns to the river in addition to groundwater mass loading.

5. Summary and conclusions

The UZF-RT3D variably-saturated multi-species reactive transport model was amended to include equilibrium chemical reactions for application to salt-affected agricultural groundwater systems. The developed Salinity Equilibrium Chemistry (SEC) module includes precipitation-dissolution, aqueous complexation, and cation exchange equilibrium reactions for the major cations and anions (calcium, magnesium, sodium, potassium, sulfate, chloride, bicarbonate, and carbonate). The module is imbedded into the UZF-RT3D modeling code to allow the fate and reactive transport of these ions to be simulated in both the unsaturated and saturated zones of an aquifer system. The resulting UZF-RT3D/SEC model also includes routines for simulation of the cycling of C, N, and S in the plant-soil system, with redox reactions and sorption included for dissolved oxygen, ammonium, nitrate, and sulfate that is amenable to regional-scale analysis of salinization. Calculation of groundwater solution temperature and pH, non-equilibrium reactions between the solid phase and the soil solution due to

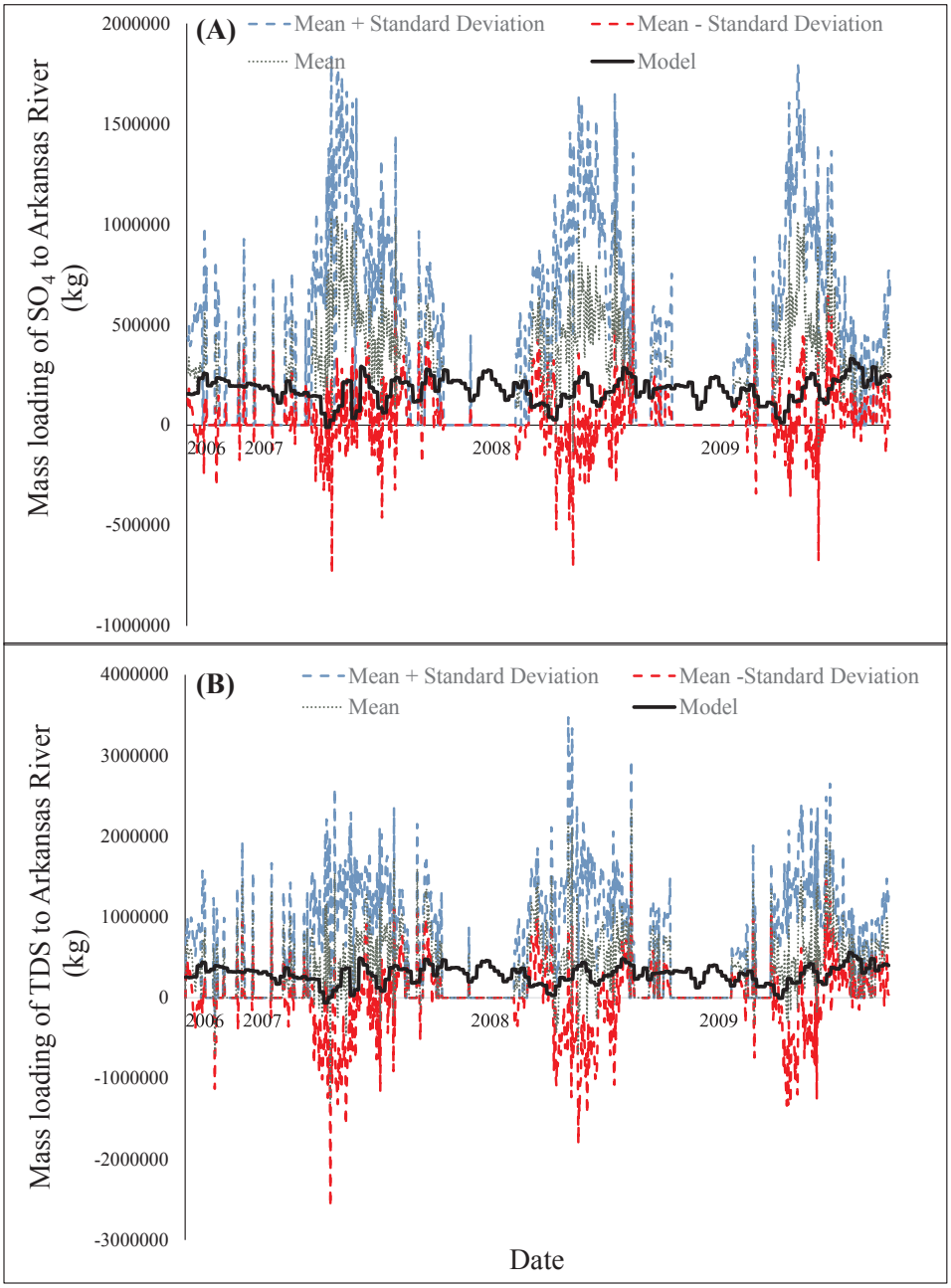

Fig. 18. Model-simulated (A) SO_4 and (B) TDS groundwater mass loading to the Arkansas River for each day during the 2006–2009 simulation period with a comparison to statistics of stochastic mass balance estimates of total unaccounted-for mass loading.

heterogeneities, effects of chemical precipitation and dissolution on soil porosity, impact of partial CO_2 pressure on the full C cycle, and consideration of high ionic strength ($I > 0.5$) were not directly considered in the current analysis. The potential effects of such processes should be examined in future model refinements.

The model is showcased in application to a 500 km^2 irrigated groundwater system along the Lower Arkansas River alluvial aquifer system in southeastern Colorado, with model results tested against a large dataset of observed salt concentrations and estimates of groundwater salt ion mass loading to the river. Findings indicate that including the SEC module results in simulated salt ion concentration values that approach the high concentrations observed in the study region, addressing a deficiency noted by Tavakoli Kivi and Bailey (2017) in their earlier modeling of sulfur and the sulfate ion in the Arkansas River Valley using UZF-RT3D. Of key importance is the ability of the model to reasonably predict over a broad landscape not only groundwater salt concentrations but also soil salinity, which can be used to determine impact on crop yield along with loadings to the river network, which affect downstream irrigated areas. The fully-calibrated model now can be used to investigate best management practices for salt remediation in the Colorado's Lower Arkansas River Valley and shows potential for application to similar salt-affected regions worldwide.

Acknowledgments

This study was made possible by the cooperative assistance of more than 120 landowners in Colorado's Lower Arkansas River Basin and by numerous water agencies. Major financial support was provided by grants from the US Agency for International Development through the US-Pakistan Center for Advanced Studies in Water (10035947-S1), the National Integrated Water Quality Program of the USDA National Institute of Food and Agriculture (2014-51130-22491), the Colorado

Department of Public Health and Environment (PO FAA WQC1349262), the Colorado Agricultural Experiment Station (COL00684), the Southeastern Colorado Water Conservancy District, the Lower Arkansas Valley Water Conservancy District, and the United States Bureau of Reclamation (R09AP60007). The views and conclusions contained in this document are those of the authors and should not be interpreted as representing the opinions or policies of the government of Colorado or the US government.

Appendix A. Supplementary data

Supplementary data to this article can be found online at https://doi.org/10.1016/j.jhydrol.2019.02.040.

References

Allison, J., Kevin, J., 1991. MINTEQA2: A geochemical assessment model for environmental systems: Version 3.0 User's manual. Technical Report. 600/3-91/021.
Al-Hamdan, A.Z., Reddy, K.R., 2008. Electrokinetic remediation modeling incorporating geochemical effects. J. Geotech. Geoenviron. Eng. 134, 91–105.
Appelo, C.A.J., Postma, D., 2005. Geochemsitry, Groundwater and Pollution. Taylor & Francis Group.
Ayers, R.S., Westcot, D.W., 1985, Water Quality for Agriculture, FAO Irrigation and Drainage Paper 29 rev 1. FAO, UN, Rome 174pp.
Bailey, R.T., Morway, E.D., Niswonger, R., Gates, T.K., 2013a. Modeling variably saturated multispecies reactive groundwater solute transport with MODFLOW-UZF and RT3D. Groundwater 51 (5), 752–761.
Bailey, R.T., Gates, T.K., Halvorson, A.D., 2013b. Simulating variably-saturated reactive transport of selenium and nitrogen in agricultural groundwater systems. J. Contam. Hydrol. 149, 27–45.
Bailey, R.T., Gates, T.K., Ahmadi, M., 2014. Simulating reactive transport of selenium coupled with nitrogen in a regional-scale irrigated groundwater system. J. Hydrol. 515, 29–46.
Bailey, R.T., Gates, T.K., Romero, E.C., 2015. Assessing the effectiveness of land and water management practices on nonpoint source nitrate levels in an alluvial stream-aquifer system. J. Contam. Hydrol. 179, 102–115.
Barry, D.A., Bajracharya, K., Crapper, M., Prommer, H., Cunningham, C.J., 2000. Comparison of split-operator methods for solving coupled chemical non-equilibrium reaction/groundwater transport models. Math Comput Simul 53 (1–2), 113–127.
Blanco, R.I., Naja, G.M., Rivero, R.G., Price, R.M., 2013. Spatial and temporal changes in groundwater salinity in South Florida. Appl. Geochem. 38, 48–58.
Brier, G.W., 1950. Verification of forecasts expressed in terms of probability. Monthly Weather Rev. 78 (1–3).
Burkhalter, J.P., Gates, T.K., 2005. Agroecological impacts from salinization and waterlogging in an Irrigated river valley. J. Irrig. and Drain. Eng. 131 (2), 197–209.
Burkhalter, J.P., Gates, T.K., 2006. Evaluating regional solutions to salinization and waterlogging in an irrigated river valley. J. Irrig. Drain. Eng. 132 (1), 21–30.
Case, D.H., Wang, F., Giammar, D.E., 2011. Precipitation of magnesium carbonates as a function of temperature, solution composition, and presence of a silicate mineral substrate. Environ. Eng. Sci. 28 (12), 881–889.
Carrayrou, J., Mose, R., Behra, P., 2004. Operator-splitting procedures for reactive transport and comparison of mass balance errors. J Contam. Hydrol. 68 (3–4), 239–268.
Chen, W., Hou, Z., Wu, L., Liang, Y., Wei, C., 2010. Evaluating salinity distribution in soil irrigated with saline water in arid regions of northwest China. Agric. Water Manage. 97 (12), 2001–2008.
Crawford, J., 1999, Geochemical modelling – a review of current capabilities and future directions. Department of Chemical Engineering and Technology, Division of Chemical Engineering, Royal Institute of Technology, Stockholm.
Doherty, J., 2007. PEST User Manual, fifth edition. Watermark Numerical Computing, Brisbane, Queensland, Australia.
Ebrahimi, M., Kazemi, H., Ehtashemi, M., Rockaway, T., 2016. Assessment of groundwater quantity and quality and saltwater intrusion in the Damghan basin, Iran, Chemie der Erde. Geochemistry 76 (2), 227–241.
Ezzedine, S. 2015, Overview of geochemical modeling for geothermal energy: model description and uncertainty quantification. In: Proc. 40th Workshop on Geothermal Reservoir Engineering, Standord Univ., California.
Farid, I., Zouari, K., Rigane, A., Beji, R., 2015. Origin of the groundwater salinity and geochemical processes in detrital and carbonate aquifers: case of Chougafiya basin (Central Tunisia). J. Hydrol. 530, 508–532.
Frind, E.O., Duynisveld, W.H.M., Strebel, O., Boettcher, J., 1990. Modeling of multi-component transport with microbial transformation in groundwater: the Fuhrberg case. Water Resour. Res. 26 (8), 1707–1719.
Forkutsa, I., Sommer, R., Shirokova, Y.I., Lamers, J.P.A., Kienzler, K., Tischbein, B., Martius, C., Vlek, P.L.G., 2009. Modeling irrigated cotton with shallow groundwater in the Aral Sea Basin of Uzbekistan: II. Soil salinity dynamics. Irrig. Sci. 27 (4), 319–330.
Gates, T.K., Burkhalter, J.P., Labadie, J.W., Valliant, J.C., Broner, I., 2002. Monitoring and modeling flow and salt transport in a salinity-threatened irrigated valley. J. Irrig. Drain. Eng. 128 (2), 88–99.
Gates, T.K, Steed, G.H., Niemann, J.D., Labadie, J.W., 2016. Data for Improved Water Management in Colorado's Arkansas River Basin. Hydrological and Water Quality Studies, Colorado State University.
Gates, T.K., Cox, J.T., Morse, K.C., 2018. "Uncertainty in mass-balance estimates of regional irrigation-induced return flows and pollutant loads to a river". J. Hydrol. Reg. Stud. 19, 193–210.
Goff, K., Lewis, M.E., Person, M.A., Konikow, L.F., 1998. Simulated effects of irrigation on salinity in the Arkansas River Valley in Colorado. Ground Water 36, 76–86.
Gonçalves, M.C., Šimůnek, J., Ramos, T.B., Martins, J.C., Neves, M.J., Pires, F.P., 2006. Multicomponent solute transport in soil lysimeters irrigated with waters of different quality. Water Resour. Res. 42, W08401. https://doi.org/10.1029/2006WR004802, 17 pp.
Grieve, C.M., Grattan, S.R., Maas, E.V., 2012. Plant salt tolerance. Chap. 13 in Wallender, W.W., Tanji, K.K., Agricultural salinity assessment and management. 2nd ed. Manuals and Reports on Engineering Practice No. 71, Amer. Soc. Civil Engineers, Reston, VA.
Harbaugh, A.W., 2005, MODFLOW-2005, the US Geological Survey modular groundwater model: the ground-water flow process (p. 253). Reston, VA: US Department of the Interior, US Geological Survey.
Harrington, N., Cook, P., 2014, Groundwater in Australia, National Centre for Groundwater Research and Training, Australia.
Haynes, W.M., 2016. Handbook of Chemistry and Physics. CRC Press, Boca Raton, FL.
Herczeg, A.L., Dogramaci, S.S., Leanet, F.W.J., 2001. Origin of dissolved salts in a large, semi-arid groundwater system: Murray Basin, Australia. Mar. Freshwater Res. 52, 41–52.
Hukkinen, J., 1993. Institutional distortion of drainage modeling in Arkansas River Basin. J. Irrig. Drain. Eng. 119, 743–755.
Huyakorn, P.S., Kool, J.B., Wu, Y.S., 1991, VAM2D-Variably saturated analysis model in two dimensions.Version 5.2 with hysteresis and chained decay transport. Documentation and user's guide. NUREG/CR-5352, Rev. 1. U.S. Nuclear Regulatory Commission, Washington, DC.
Jacques, D., Šimůnek, J., 2005, Multicomponent – Variable Sat- urated Transport Model, Description, Manual, Verification and Examples, Waste and Disposal. SCKoCEN, BLG-998, Mol, Belgium.
Jacques, D., Šimůnek, J. Mallants, D., van Genuchten, M. Th., 2003, The HYDRUS-PHREEQC Multicomponent Transport Model for Variably-Saturated Porous Media: Code Verification and Application. In: MODFLOW and More 2003: Understanding through modeling, E. Poeter, Ch. Zheng, M. Hill, and J. Doherty (Editors). Int. Ground Water Modeling Center, Colorado School of Mines, FOG Collins, Colorado, pp, 23–27.
Jalali, M., 2007. Salinization of groundwater in arid and semi-arid zones: an example from Tajarak, western Iran. Environ. Geol. 52 (6), 1133–1149.
Jamshidzadeh, Z., Mirbagheri, S.A., 2011. Evaluation of groundwater quantity and quality in the Kashan Basin, Central Iran. Desalination 270 (1–3), 23–30.
Javadi, A., Al-Najjar, M., 2007. Finite element modeling of contaminant transport in soils including the effect of chemical reactions. J. Hazard. Mater. 143 (3), 690–701.
Jeevanandam, M., Kannan, R., Srinivasalu, S., and Rammohan, V., 2007, Hydrogeochemistry and Groundwater Quality Assessment of Lower Part of the Ponnaiyar River Basin, Cuddalore District, South India, Environmental Monitoring and Assessment, Volume 132, Issue 1, pp 263–274.
Konikow, L.F., 2011. The secret to successful solute-transport modeling. Ground Water 49 (2), 144–159.
Krumgalz, B.S., 2017. Temperature dependence of mineral solubility in water. Part I. alkaline and alkaline earth chlorides. J. Phys. Chem. Ref. Data 46 (4), 043101.
Konikow, L.F., Person, M., 1985. Assessment of long-term salinity changes in an irrigated stream aquifer system. Water Resour. Res. 21, 1611–1624.
Latif, M., Ahmad, M.Z., 2009. Groundwater and soil salinity variation in a canal command area in Pakistan. Irrig. Drain. 58, 456–468.
Lin, Y.W., Garcia, L.A., 2008. Development of a hydro-salinity simulation model for Colorado's Arkansas Valley. J. Irrig. Drain. Eng. 134, 757–767.
Lorenzen, G., Sprenger, C., Baudron, P., Gupta, D., Pekdeger, A., 2012. Origin and dynamics of groundwater salinity in the alluvial plains of western Delhi and adjacent territories of Haryana State. India. Hydrolog. Proc. 26 (15), 2333–2345.
Lucia, A., Henley, H., Thomas, E., 2015. Multiphase equilibrium flash with salt precipitation in systems with multiple salts. Chem. Eng. Res. Des. 93, 662–674.
Mahmood, K., Morris, J., Collopy, J., Slavich, P., 2001. Groundwater uptake and sustainability of farm plantations on saline sites in Punjab province, Pakistan. Agric. Water Manage. 48 (1), 1–20.
Merkel, B.J., Planer-Friedrich, B., Nordstrom, D.K., 2005. Groundwater geochemistry. A Practical Guide to Modeling of Natural and Contaminated Aquatic Systems, 2.
Miller, C.W., Benson, L.V., 1983. Simulation of solute transport in a chemically reactive heterogeneous system: model development and application. Water Resour. Res. 19 (2), 381–391.
Millero, F.J., 2001. The physical chemistry of natural waters. Wiley.
Misra, A.K., Mishra, A., 2007. Study of quaternary aquifers in Ganga Plain, India: focus on groundwater salinity, fluoride and fluorosis. J. Hazard. Materials 144 (1), 438–448.
Morway, E.D., Gates, T.K., 2012. Regional assessment of soil water salinity across an intensively irrigated river valley. J. Irrig. Drain. Eng. 138 (5), 393–405.
Morway, E.D., Gates, T.K., Niswonger, R.G., 2013. Appraising options to reduce shallow groundwater tables and enhance flow conditions over regional scales in an irrigated alluvial aquifer system. J. Hydrol. 495, 216–237.
Narasimhan, T.N., White, A.F., Tokunaga, T., 1986. Groundwater contamination from an inactive uranium mill tailings pile, 2, Application of a dynamic mixing model. Water Resour. Res. 22 (13), 1820–1834.
Niswonger, R.G., Prudic, D.E., Regan, R.S., 2006. Documentation of the unsaturated zone flow (UZF1) Package for Modeling Unsaturated flow Between the Land Surface and the Water Table with MODFLOW-2005. U.S Geol. Surv. Tech. Methods 6–A19.
Niswonger, R.G., Panday, S., Motomu, I., 2011, MODFLOW-NWT, A Newton Formulation for MODFLOW-2005: U.S. Geological Survey Techniques and Methods 6-A37, 44p.

Oosterbaan, R.J., 2005, SAHYSMOD (version 1.7a), Description of principles, user manual and case studies, International Institute for Land Reclamation and Improvement, Wageningen, Netherlands, 140.
Panthi, S.R., 2003, April. Carbonate chemistry and calcium carbonate saturation state of rural water supply projects in Nepal. In: Proceedings of the Seventh International Water Technology Conference, Cairo, Egypt, pp. 1–3.
Parkhust, D.L., Appelo, C.A.J., 2013, Description of Input and Examples for PHREEQC Version 3 – A Computer Program for Speciation, Batch-Reaction, One-Dimensional Transport, and Inverse Geocehmical Calculations, Chapter 43 of Section A, Groundwater, Book 6, Modeling Techniques.
Parkhurst, D.L., Kipp, K.L., Engesgaard, Peter, Charlton, S.R., 2004. PHAST—a program for simulating ground-water flow, solute transport, and multicomponent geochemical reactions. U.S Geol. Surv. Techniq. Method 6–A8, 154 p.
Parkhust D.L., Appelo, C.A.J., 1999, User's guide to PHREEQC (Version-2)-a computer program for speciation, batch-reaction, one-dimensional transport, and inverse geochemical calculations, USGS, Report 99(4259), 326.
Pauwels, H., Kloppmann, W., Foucher, J.C., Martelat, A., Fritsche, V., 1998. Field tracer test for denitrification in a pyrite-bearing schist aquifer. Appl. Geochem. 13 (6), 767–778.
Paz-Garcia, J.M., Johannesson, B., Ottosen, L., Ribeiro, A., Rodríguez-Maroto, J.M., 2013. Computing multi-species chemical equilibrium with an algorithm based on the reaction extents. Comput. Chem. Eng. 58, 135–143.
Pereira, L.S., Goncalves, J.M., Dong, B., Mao, Z., Fang, S.X., 2007. Assessing basin irrigation and scheduling strategies for saving irrigation water and controlling salinity in the upper Yellow River Basin, China. Agric. Water Manage. 93 (3), 109–122.
Pillay, V., Gärtner, R.S., Himawan, C., Seckler, M.M., Lewis, A.E., Witkamp, G.J., 2005. $MgSO_4$ + H_2O system at eutectic conditions and thermodynamic solubility products of $MgSO_4{\cdot}12H_2O$ (s) and $MgSO_4{\cdot}7H_2O$ (s). J. Chem. Eng. Data 50 (2), 551–555.
Plummer, L.N., Busenberg, E., 1982. The solubilities of calcite, aragonite and vaterite in CO_2-H_2O solutions between 0 and 90 C, and an evaluation of the aqueous model for the system $CaCO_3$-CO_2-H_2O. Geochim. Cosmochim. Acta 46 (6), 1011–1040.
Postma, D., Boesen, C., Kristiansen, H., Larsen, F., 1991. Nitrate reduction in an unconfined sandy aquifer: water chemistry, reduction processes, and geochemical modeling. Water Resour. Res. 27 (8), 2027–2045.
Piper, A.M., 1944. A graphical procedure in the geochemical interpretation of water-analysis. Eos. Tran. Am. Geophys. Union 25 (6), 914–928.
Prommer, H., Barry, D.A., Zheng, C., 2003. MODFLOW/MT3DMS-based reactive multicomponent transport modeling. Groundwater 41 (2), 247–257.
Qureshi, A.S., McCornick, P.G., Qadir, M., Aslam, Z., 2008. Managing salinity and waterlogging in the Indus Basin of Pakistan. Agric. Water Manage. 95 (1), 1–10.
Rasouli, F., Pouya, A.K., Šimůnek, J., 2013. Modeling the effects of saline water use in wheat-cultivated lands using the UNSATCHEM model. Irrig. Sci. 31 (5), 1009–1024.
Robbins, C.W., Jurinak, J.J., Wagenet, R.J., 1980. Calculating cation exchange in a salt transport model 1. Soil Sci. Soc. Am. J. 44 (6), 1195–1200.
Rubin, J., 1983. Transport of reacting solutes in porous media: Relation between mathematical nature of problem formulation and chemical nature of reactions. Water Resour. Res. 19 (5), 1231–1252.
Schoups, G., Hopmans, J.W., Young, C.A., Vrugt, J.A., Wallender, W.W., Tanji, K.K., Panday, S., 2005. Sustainability of irrigated agriculture in the San Joaquin Valley, California. PNAS 102 (43), 15352–15356.
Schoups, G., Hopmans, J.W., Tanji, K.K., 2006. Evaluation of model complexity and space–time resolution on the prediction of long-term soil salinity dynamics, western San Joaquin Valley, California. Hydrol. Proc. 20 (13), 2647–2668.
Shammas, M.I., Jacks, G., 2007. Seawater intrusion in the Salalah plain aquifer, Oman. J. Environ. Hydrol., Volume 15 Paper 19.
Sherif, M., Mohamed, M., Kacimov, A., Shetty, A., 2011. Assessment of groundwater quality in the northeastern coastal area of UAE as precursor for desalination. Desalination 273 (2–3), 436–446.
Shultz, C.D., Bailey, R.T., Gates, T.K., Heesemann, B.E., Morway, E.D., 2018. Simulating selenium and nitrogen fate and transport in coupled stream-aquifer systems of irrigated regions. J. Hydrol. 560, 512–529.
Singh, A., Panda, S.N., 2012. Integrated salt and water balance modeling for the management of waterlogging and salinization; I: Validation of SAHYSMOD. J. Irrig. Drain. Eng. 138, 955–963.
Singh, N.T., 2005. Irrigation and soil salinity in the Indian subcontinent: Past and present. Lehigh Univ. Press, Bethlehem, PA.
Šimůnek, J., Šejna, M., van Genuchten, M. Th., 2012. The UNSATCHEM Module for HYDRUS (2D/3D) Simulating Two-Dimensional Movement of and Reactions Between Major Ions in Soils, Version 1.0, PC Progress, Prague, Czech Republic, 54 pp.
Šimůnek, J., Šejna, M., Van Genuchten, M. Th., 2005. HYDRUS-1D, version 4.14, code for simulating the one-dimensional movement of water, heat, and multiple solutes in variably saturated porous media, Tech. rep. University of California Riverside.
Šimůnek, J., Suarez, D.L., 1994. Two-dimensional transport model for variably saturated porous media with major ion chemistry. Water Resour. Res. 30 (4), 1115–1133.
Skrzypek, G., Dogramaci, S., Grierson, P.F., 2013. Geochemical and hydrological processes controlling groundwater salinity of a large inland wetland of northwest Australia. Chem. Geol. 357, 164–177.
Steefel, C.I., Lasaga, A.C., 1994. A coupled model for transport of multiple chemical species and kinetic precipitation/dissolution reactions with application to reactive flow in single phase hydrothermal systems. Am. J. Sci. 294 (5), 529–592.
Steefel, C.I., Appelo, C.A.J., Arora, B., Jacques, D., Kalbacher, T., Kolditz, O., Lagneau, V., Lichtner, P.C., Mayer, K.U., Meeussen, J.C.L., Molins, S., 2015. Reactive transport codes for subsurface environmental simulation. Computat. Geosci. 19 (3), 445–478.
Tafteh, A., Sepaskhah, A.R., 2012. Application of HYDRUS-1D model for simulating water and nitrate leaching from continuous and alternate furrow irrigated rapeseed and maize fields. Agri. Water Manage. 113, 19–29.
Tweed, S.O., Leblanc, M., Webb, J.A., Lubczynski, M.W., 2007. Remote sensing and GIS for mapping groundwater recharge and discharge areas in salinity prone catchments, southeastern Australia. Hydrogeo. J. 15 (1), 75–96.
Tavakoli Kivi, S., Bailey, R.T., 2017. Modeling sulfur cycling and sulfate reactive transport in an agricultural groundwater system. Agric. Water Manage. 185 (1), 78–92.
Truesdell, A.H., Jones, B.F., 1974. WATEQ-a computer program for calculating chemical equilibrium for natural waters. US Geological Survey.
Tuteja, N.K., Beale, G., Dawes, W., Vaze, J., Murphy, B., Barnett, P., Rancic, A., Evans, R., Geeves, G., Rassam, D., Miller, M., 2003. Predicting the effects of landuse change on water and salt balance—a case study of a catchment affected by dryland salinity in NSW Australia. J. Hydrol. 283, 67–90.
Wagenet, R.J., Hutson, J.L., 1987, LEACHM-Leaching estimation and chemistry model. Center Environ. Res., Cornell Univ., Ithaca, NY.
Wang, Y., Deng, C., Liu, Y., Niu, Z., Li, Y., 2018. Identifying change in spatial accumulation of soil salinity in an inland river watershed. Sci. Total Environ. 621, 177–185.
Walsh, M.P., Bryant, S.L., Schechter, R.S., Lake, L.W., 1984. Precipitation and dissolution of solids attending flow through porous media. AIChE J. 30 (2), 317–328.
Yeh, G.T., Tripathi, V.S., 1989. A critical evaluation of recent developments in Hydrogeochemical transport models of reactive multichemical components. Water Resor. Res. 25 (2), 93–108.
Yeh, G.T., Tripathi, V.S., Gwo, J.P., Cheng, H.P., Cheng, J.C., Salvage, K.M., Li, M.H., Fang, Y., Li, Y., Sun, J.T., Zhang, F., Siegel, M.D., 2004. HYDROGEOCHEM 5.0: A Three-Dimensional Model of Fluid Flow, Thermal Transport, and HYDROGEOCHEMical Transport through Variably Saturated Conditions, Oak Ridge National Laboratory.
Zeng, Y., Li, Z., 2015. Solubility measurement and modeling for the NaCl–NH_4Cl–monoethylene glycol–H_2O system from (278 to 353) K. J. Chem. Eng. Data 60 (8), 2248–2255.